REPORT DOCUMENTATION PAGE		Form Approved OMB No. 0704-0188

The public reporting burden for this collection of information is estimated to average 1 hour per response, including the time for reviewing instructions, searching existing data sources, gathering and maintaining the data needed, and completing and reviewing the collection of information. Send comments regarding this burden estimate or any other aspect of this collection of information, including suggestions for reducing the burden, to Department of Defense, Washington Headquarters Services, Directorate for Information Operations and Reports (0704-0188), 1215 Jefferson Davis Highway, Suite 1204, Arlington, VA 22202-4302. Respondents should be aware that notwithstanding any other provision of law, no person shall be subject to any penalty for failing to comply with a collection of information if it does not display a currently valid OMB control number.
PLEASE DO NOT RETURN YOUR FORM TO THE ABOVE ADDRESS.

1. REPORT DATE *(DD-MM-YYYY)* 30-5-2008	2. REPORT TYPE Final Technical Report	3. DATES COVERED *(From - To)* 1st April 2005 to 31 Mar 2008

4. TITLE AND SUBTITLE A Theoretical Study of Leading Edge Noise	5a. CONTRACT NUMBER
	5b. GRANT NUMBER N00014-05-1-0463
	5c. PROGRAM ELEMENT NUMBER
6. AUTHOR(S) Stewart Glegg	5d. PROJECT NUMBER
	5e. TASK NUMBER
	5f. WORK UNIT NUMBER

7. PERFORMING ORGANIZATION NAME(S) AND ADDRESS(ES) Florida Atlantic University 777 Glades Road Boca Raton FL 33431	8. PERFORMING ORGANIZATION REPORT NUMBER

9. SPONSORING/MONITORING AGENCY NAME(S) AND ADDRESS(ES) Ronald R. Joslin ONR 331 Office of Naval Research 875 North Randolph Street Arlington, VA 22203-1995	10. SPONSOR/MONITOR'S ACRONYM(S)
	11. SPONSOR/MONITOR'S REPORT NUMBER(S)

12. DISTRIBUTION/AVAILABILITY STATEMENT

Approved for Public Release;
Distribution is Unlimited

13. SUPPLEMENTARY NOTES

14. ABSTRACT

The report describes a theoretical procedure for calculating leading edge noise which addresses the differences found between current theoretical calculations and wind tunnel measurements of unsteady lift on airfoils in turbulent flow. The results have been compared with experiments carried at in a companion study at Virginia Tech by Dr. William Devenport. It was concluded that the effect of angle of attack on the radiated noise is relatively weak but the effect of thickness is to reduce the radiated sound levels at high frequencies.

15. SUBJECT TERMS

Debra K. Campbell, MPA, CRA
Associate Director, Sponsored Programs
Florida Atlantic University

16. SECURITY CLASSIFICATION OF:			17. LIMITATION OF ABSTRACT	18. NUMBER OF PAGES	19a. NAME OF RESPONSIBLE PERSON
a. REPORT	b. ABSTRACT	c. THIS PAGE			
U	UU	UU	UU	40	19b. TELEPHONE NUMBER *(Include area code)* 541-297-1287

Standard Form 298 (Rev. 8/98)
Prescribed by ANSI Std. Z39.18

A THEORETICAL STUDY OF LEADING EDGE NOISE

Final Report

For

ONR Grant No. N00014-05-1-0463

Submitted by

Stewart Glegg
Dept. of Ocean Engineering
Florida Atlantic University

May 2008

20090105205

Summary

The technical objectives of this study were

- A theoretical evaluation of the effects of angle of attack on leading edge noise from airfoils
- To verify the theory in comparison with wind tunnel measurements made in a companion study at Virginia Tech

The technical approach was to develop a theoretical procedure for calculating leading edge noise which addresses the differences found between current theoretical calculations and wind tunnel measurements of unsteady lift on airfoils in turbulent flow. The results have been compared with experiments carried at in a companion study at Virginia Tech by Dr. William Devenport.

In the first part of this study the unsteady loading on an airfoil of arbitrary thickness was evaluated by using the generalized form of Blasius theorem and a conformal mapping that maps the airfoil surface onto a circle. For a blade vortex interaction the results show that the time history of the unsteady loading is determined by the passage of the vortex relative to the leading edge singularity in the circle plane. The singularity lies inside the circle and moves to a smaller radius as the thickness is increased, causing the unsteady loading pulse to be smoothed. The effect of angle of attack is to move the stagnation point relative to the leading edge singularity and this significantly increases the unsteady lift if the vortex passes on the suction side of the airfoil. These characteristics are different for a step upwash gust, which is considered as a simplified model of a large scale turbulent gust. It is shown that the time history of the magnitude of the unsteady loading is almost completely unaltered by angle of attack for the step gust, but its direction of action rotates forward by an angle equal to the angle of attack, extending an earlier result by Howe for a flat plate in a turbulent flow to airfoils of arbitrary thickness. However spectral analysis of the gust shows that the high frequency blade response is reduced as the thickness of the airfoil is increased.

The second part of this study considered the sound radiation from airfoils in a turbulent flow as a function of both thickness and angle of attack. The theoretical method for the response of a blade to an incoming gust developed in the first part of the study, or a boundary element method, was combined with a description of the turbulence spectrum to provide theoretical prediction of the radiated noise. The results were compared to wind tunnel measurements of the noise radiated from a number of different airfoils made as part of a companion study at Virginia Tech. It was concluded that the effect of angle of attack on the radiated noise is relatively weak but the effect of thickness is to reduce the radiated sound levels at high frequencies.

TABLE OF COINTENTS

Summary

PART A: Unsteady Loading on an Airfoil of Arbitrary Thickness

Part B: Sound radiation from Three Dimensional Airfoils in a Turbulent Flow

PART A: Unsteady Loading on an Airfoil of Arbitrary Thickness

1. Introduction

The unsteady loading on an airfoil caused by an incident gust is important in many applications and has received significant attention in the literature. The problem of a two dimensional flat plate airfoil in a uniform flow encountering a harmonic upwash gust was addressed by Sears [1]. Amiet and Sears [2] extended the solution to three dimensions for airfoils of large chord. Goldstein and Atassi [3] provided an asymptotic solution for a two dimensional potential flow over an airfoil of finite thickness, camber and angle of attack based on the assumptions of thin airfoil theory. Atassi [4] showed how this solution could be split into three independent terms that separated the effects of thickness, camber and angle of attack. Howe [5] gave a formula for the unsteady loading on a body of arbitrary shape based on a volume integral of a Greens function and the Lamb vector of the unsteady flow. He showed (Howe [6]) that, for a flat plate in a turbulent flow the unsteady lift was rotated forward as the angle of attack was increased. In Howe [7] it was shown that, for a stationary airfoil, the unsteady loading could be obtained using a surface integral over the body in which the integrand is a Greens function multiplied by the velocity induced by the vorticity in the flow. It was also shown (Howe [7-9]) that the unsteady loading is strongly affected by the application of the Kutta condition at the trailing edge of the airfoil. If the Kutta condition is not applied the time history of the unsteady loading exhibits a pulse as the gust passes the trailing edge. If the Kutta condition is applied, and disturbances in the wake are convected at the speed of the mean flow, then the pulse generated as the gust passes the trailing edge is completely cancelled. By ignoring the trailing edge Howe [7] showed that the unsteady blade response approximated Sears function for non dimensional frequencies $\sigma = \omega b/U > 1$, where b is the semichord, U is the free stream velocity and ω is the angular frequency of the unsteady load. Gershfeld [10] considered a turbulent gust incident on a flat plate of finite thickness and showed that the radiated sound was reduced at high frequencies as the thickness was increased. Similar results were obtained by Martinez and Rudzynsky [11] and Grace [12] for blade vortex interactions. Numerical methods such as the unsteady panel method described by Grace[12] or computational methods based on the Navier Stokes equations, as described by Lockard and Morris [13], have given the solution for the unsteady loading on airfoils of arbitrary shape.

In this paper we will show that the unsteady loading on a two dimensional airfoil in an incompressible potential flow can be obtained using the generalized form of Blasius theorem. The contribution of this approach is that it shows directly the physical impact of both thickness and angle of attack on the unsteady loading, without being limited by the assumptions of thin airfoil theory. It is shown that the characteristics of the response to a blade vortex interaction are quite different from the response to a step upwash gust. The blade vortex interaction is very sensitive to the effect of angle of attack, but this is not the case for a step gust. It is found that, for the step gust, the time history of the magnitude of the unsteady lift is almost unaltered by angle of attack, but its direction of action is rotated forward as the angle of attack is increased. This agrees with and extends Howe's

4

[6] result for a flat plate to airfoils of arbitrary thickness. However spectral analysis of the gust shows that the high frequency blade response is reduced as the thickness of the airfoil is increased.

2. Unsteady loading on an airfoil

2.1 The unsteady flow

The unsteady loading will be calculated for a gust incident on an airfoil at rest in a uniform mean flow. The fluid will be assumed to be inviscid, incompressible and two dimensional so the unsteady loading can be obtained from potential flow theory. The complex potential of the flow is defined as $W(Z)$, (where $Z=X+iY$ and (X,Y) represents a point in the physical plane), and can be obtained by mapping the airfoil surface onto a circle in the complex z-plane using the transformation

(1)

$$Z = (z - \lambda) + (a - \lambda)^2 / (z - \lambda) \qquad (z - \lambda) = Z/2 + \sqrt{Z^2/4 - (a - \lambda)^2},$$

where a is the radius of the circle and λ is a lengthscale to be defined below. For a Joukowski airfoil at an angle of attack α, in a flow with uniform speed U, the complex potential is given (see for example Acheson[14]) as

(2)

$$W_o(Z) = w_o(z) = Uze^{-i\alpha} + \frac{Ua^2e^{i\alpha}}{z} - \frac{i\Gamma}{2\pi}\ln(z),$$

where the airfoil chord is $4a^2/(a+\lambda)$ and its thickness to chord ratio is given by $3\sqrt{3}\lambda(a+\lambda)/(4a^2)$. For thin airfoils $\lambda<<1$ the chord is approximately $4a$ and the blade thickness to chord ratio is 5.2λ. The surface of the airfoil is defined by the circle of radius a in the z plane centered at $z=0$ and the trailing edge of the airfoil lies at $z=a$. To satisfy the Kutta condition the mean circulation about the airfoil is given by $\Gamma = -4\pi Ua\sin\alpha$.

To calculate the unsteady loading on the airfoil we will consider the incident gust to be a point vortex of strength γ_0 that is convected with the mean flow. Howe [8] has shown that the response of the airfoil to an incident vortex is equivalent to the harmonic gust problem considered by Sears [1] and Goldstein and Atassi [3]. These results assume Rapid Distortion Theory (RDT), (Batchelor and Proudman [15], Hunt [16], Goldstein [17]) which requires that the vortex is convected by the mean flow without being displaced by its image vortex inside the airfoil. This assumption cannot be applied for a vortex which is convected along the stagnation streamline upstream of the leading edge because the vortex will come rest at the stagnation point. However this is not realizable for a vortex with non-zero strength because the image vorticity will displace the vortex from the stagnation point and it will then be convected by the adjacent flow. The issue of gust distortion next to the stagnation point can lead to numerical errors for harmonic gust descriptions (Atassi and Grzedzinski [18]) but these are avoided by describing the incident gust as a point vortex providing it is not located precisely on the stagnation streamline.

5

In this analysis we will assume Rapid Distortion Theory which requires that the vortex is convected by the mean flow along a streamline without change in strength and we will avoid the issue of gust distortion at the stagnation point by not placing a vortex on the stagnation streamline in numerical calculations. The vortex position is then relatively easy to calculate and will by specified as $z_o(t)$ in the circle plane. The velocity potential induced by the vortex and its image inside the circle is then

(3)

$$w_v(z,t) = -\frac{i\gamma_o}{2\pi}\ln(z-z_o) + \frac{i\gamma_o}{2\pi}\ln(z_I - z) - \frac{i\gamma_o}{2\pi}\ln(z/z_o^*),$$

where $z_I = a^2/z_o^*$ is the location of the image vortex. The potential specified in (3) satisfies the non penetration boundary condition on the airfoil surface but does not satisfy the Kutta condition. This can be achieved by introducing a vorticity distribution in the wake downstream of the trailing edge which ensures that the unsteady velocity at the trailing edge is finite. If the potential induced by the wake is $w_w(z,t)$ then the unsteady Kutta condition requires that $w_v'(a,t) + w_w'(a,t) = 0$, where the prime represents a derivative with respect to the complex variable z. The wake will be assumed to lie on the x-axis in the circle plane so the velocity potential induced by the wake is

(4)

$$w_w(z,t) = \frac{-i}{2\pi}\int_{-\infty}^{t}\mu(\tau)\{\ln(z - x_w(t,\tau)) - \ln(x_I(t,\tau) - z)\}d\tau,$$

where $\mu(\tau)$ is the rate of change of vorticity at the trailing edge at time τ, $x_w(t,\tau)$ is the location of the vorticity at time t generated at the trailing edge at time τ and $x_I = a^2/x_w$. Note that $x_w(t,\tau) > x_w(\tau,\tau) = a + \varepsilon$ when $\tau < t$ and the small parameter $\varepsilon > 0$ ensures that the wake is initiated downstream of the trailing edge. To satisfy the Kutta condition we require that $w_v'(a,t) + w_w'(a,t) = 0$ and using Eq. (4) we obtain

(5)

$$w_v'(a,t) = \frac{i}{2\pi}\int_{-\infty}^{t}\mu(\tau)\left(\frac{1}{(a-x_w)} - \frac{1}{(a-x_I)}\right)d\tau = \frac{i}{2\pi}\int_{-\infty}^{t}\mu(\tau)\left(\frac{x_w + a}{a(a-x_w)}\right)d\tau \quad .$$

Using Eq. (3) and Eq. (5) we obtain an integral equation for the vorticity in the wake as

(6)

$$\int_{-\infty}^{t}\mu(\tau)\left(\frac{x_w + a}{x_w - a}\right)d\tau = -\gamma_o\left(\frac{a}{(z_o - a)} + \frac{a}{(z_o^* - a)}\right).$$

This integral can be solved by standard methods using Fourier transforms and will be discussed in more detail below. However it is worth noting here that $\mu(\tau)$ is real valued.

2.2 The unsteady loading

The unsteady loading on the airfoil can be calculated from the generalized form of Blasius theorem

$$F_X + iF_Y = \left(\frac{i\rho}{2} \oint_C \left(\frac{dW}{dZ} \right)^2 dZ \right)^{\cdot} - i\rho \frac{d}{dt} \oint_C W(Z)dZ,$$

where the contour integral is carried out over the surface of the airfoil. The first integral represents the contribution from the circulation and will be represented by $(F_X + iF_Y)_c$. In steady flow the integral is evaluated (Acheson[14]) by expanding the contour onto a circle with a large radius and then using a Laurent expansion to represents the integrand. This leads to the conclusion that the load due to circulation is given by $-i\rho\Gamma U exp(i\alpha)$. However in unsteady flow the expansion of the contour to a large radius must take into account the vorticity in the wake and the presence of the vortex at Z_o. The same contour at a large radius can be used but the result must be modified by adding the contributions from the vortex and the wake. Since the wake does not support a discontinuity in pressure the contour C used in both integrals in Eq. (7) can be extended to enclose the wake without changing the value of $F_X + iF_Y$. We can draw this extension from the suction side of the trailing edge, along the upper surface of the wake to a circular contour of large radius, and then along the lower side of the wake to the lower surface of the trailing edge. The contour must be indented to bypass the singularity at the vortex located at Z_o. The circulation load can then be defined by the combination of two contour integrals as

(8)

$$(F_X + iF_Y)_c = \left(\frac{i\rho}{2} \left\{ \oint_{C_1} - \oint_{C_2} \right\} \left(\frac{dW}{dZ} \right)^2 dZ \right)^{\cdot}.$$

The path C_1 represents a circular contour of a large radius (but not so large that the starting vortex is inside the contour) centered at the origin, and the C_1 contour integral can be evaluated using a Laurent series as before. The result will be given by the total circulation, including the contributions from the vortex and its images inside the surface, which sum to γ_o, and the wake vorticity and its image, which sum to zero. The net contribution to the circulation load will be $-i\rho(\Gamma + \gamma_o)U exp(i\alpha)$. The contour C_2 represents a contour around the vortex at Z_o and can be collapsed onto a small circle centered on the vortex location where we can represent the integrand as

(9)

$$\left(\frac{dW}{dZ} \right)^2 = \left(\frac{dW_e(Z_o)}{dZ} - \frac{i\gamma_o}{2\pi(Z - Z_o)} \right)^2,$$

where $W_e(Z_o)$ represents the complex potential at Z_o from all sources but the vortex itself. Using Rapid Distortion Theory implies that $dW_e(Z_o)/dZ$ is well approximated by the steady flow at Z_o and so the integral over C_2 yields a contribution to the circulation load of $i\rho\gamma_o V(Z_o)$. The net circulation load is then given by

(10)

$$(F_X + iF_Y)_c = -i\rho\Gamma U e^{i\alpha} + i\rho\gamma_o (V(Z_o) - U e^{i\alpha}).$$

The first term represents the steady load and the second gives the contribution to the unsteady load from the vortex attraction to the surface.

The second integral in Eq. (7) represents the added mass which will be identified by $(F_X+iF_Y)_m$. The integrand can be transformed to the z plane and the contour carried out over the circle representing the surface of the airfoil and the extension enclosing the wake, giving

(11)

$$(F_X + iF_Y)_m = -i\rho \oint_C \frac{\partial w(z,t)}{\partial t} \frac{dZ}{dz} dz .$$

First we will consider the case when there is no wake, and the Kutta condition is not satisfied, so the only contribution to this integral is from the potential induced by the vortex (Eq. (3)), which gives

(12)

$$\frac{\rho \gamma_o}{2\pi} \oint_C (1 - \frac{(a-\lambda)^2}{(z-\lambda)^2}) \left(\frac{1}{(z-z_o)} \frac{dz_o}{dt} - \frac{1}{(z-z_l)} \frac{dz_l}{dt} + \left(\frac{1}{z_o} \frac{dz_o}{dt} \right)^{\bullet} \right) dz .$$

Using the residue theorem to evaluate the integral and including the contributions from the second order pole at $z=\lambda$ and the simple pole at $z=z_l$ gives the unsteady load due to the motion of the vortex as

(13)

$$\left(F_x + iF_y\right)_v = i\rho \gamma_o \left\{ \frac{(a-\lambda)^2}{(z_o-\lambda)^2} \left(\frac{dz_o}{dt} \right) - \left(\frac{dz_l}{dt} \right) \right\} = i\rho \gamma_o \left\{ \frac{(a-\lambda)^2}{(z_o-\lambda)^2} \left(\frac{dz_o}{dt} \right) + \left(\frac{a^2}{z_o^2} \frac{dz_o}{dt} \right)^{\bullet} \right\} .$$

The time history of the unsteady loading described by Eq. (13) is clearly determined by the rate of vortex convection which can be specified using $V(Z_o)$ as

(14)

$$\frac{dz_o}{dt} = \frac{dz_o}{dZ_o} \frac{dZ_o}{dt} = \frac{V(Z_o)}{1 - (a-\lambda)^2 / (z_o - \lambda)^2} .$$

This has two peaks which occur when the vortex is at it's closest point to the leading or trailing edge singularities located at $z_o=2\lambda-a$ and $z_o=a$. The time history of the unsteady load given by Eq. (13) will therefore have a leading and trailing edge pulse, which can be conveniently identified by expanding the first term in Eq. (13) using partial fractions to give

(15)

$$\left(\frac{a-\lambda}{z_o-\lambda} \right)^2 \frac{dz_o}{dt} = \frac{1}{2} \left(\frac{-(a-\lambda)V(Z_o)}{z_o+a-2\lambda} + \frac{(a-\lambda)V(Z_o)}{z_o-a} \right) .$$

8

The first term represents the leading edge pulse while the second term represents the trailing edge pulse. The magnitude of these pulses will be discussed in more detail in section 3.

To calculate the unsteady loading we must also include the added mass induced by the wake, which can be obtained from Eq. (11) using

$$\left(F_x + iF_y\right)_w = -i\rho \oint_C (1 - \frac{(a-\lambda)^2}{(z-\lambda)^2}) \frac{\partial w_w}{\partial a} dz,$$

(16)

where

$$\frac{\partial w_w}{\partial a} = \frac{i}{2\pi} \int_{-\infty}^{t} \mu(\tau) \left\{ \frac{1}{(z-x_w)} \frac{\partial x_w}{\partial a} - \frac{1}{(z-x_l)} \frac{\partial x_l}{\partial a} \right\} d\tau + \frac{\mu(t)}{2}.$$

(17)

Applying the residue theorem to Eq. (16) over the contour which encloses both the airfoil surface and the wake gives a solution which only depends on the simple poles at $z=x_w$ and $z=x_l$. The unsteady load from the wake is then

$$\left(F_x + iF_y\right)_w = i\rho \int_{-\infty}^{t} \mu(\tau) \left\{ 1 + \frac{a^2}{x_w^2} \right\} \frac{\partial x_w}{\partial a} d\tau.$$

(18)

The integral in Eq. (18) clearly depends on the rate at which vorticity is convected in the wake. There has been much debate (see Howe [9]) about the choice of convection speed and so we will proceed by allowing this to be a variable for the time being. In the Z plane the wake convection velocity will be assumed to be $V(X_w)$ and so the convection velocity in the z plane is

$$\frac{dx_w}{dt} = \frac{dx_w}{dX_w} \frac{dX_w}{dt} = \frac{V(X_w)}{1 - (a-\lambda)^2 /(x_w - \lambda)^2},$$

(19)

and it follows that

$$\left(F_x + iF_y\right)_w = i\rho \int_{-\infty}^{t} \mu(\tau) \left(\left\{ 1 + \frac{a^2}{x_w^2} \right\} \frac{(x_w - \lambda)^2 V(X_w)}{(x_w - \lambda)^2 - (a-\lambda)^2} \right) d\tau.$$

(20)

The unsteady loading is then given by the sum of Eq. (10), Eq. (13) and Eq. (20) which may be combined as

9

$$\left(F_x + iF_y\right)_u = i\rho\gamma_o\left\{\frac{(a-\lambda)^2}{(z_o-\lambda)^2}\left(\frac{dz_o}{dt}\right)+\left(\frac{a^2}{z_o^2}\frac{dz_o}{dt}\right)^{\bullet}+V(Z_o)-Ue^{i\alpha}\right\}$$
$$+i\rho\int_{-\infty}^{t}\mu(\tau)V(X_w)\left(\left\{1+\frac{a^2}{x_w^2}\right\}\frac{(x_w-\lambda)^2}{(x_w-\lambda)^2-(a-\lambda)^2}\right)d\tau$$

The first term in Eq. (21) is easily calculated from the location and velocity of the vortex. The second term however depends on the time history of the wake vorticity and requires the evaluation of a convolution integral. It will be shown in the appendix how this can be carried out using Fast Fourier Transforms.

Eq. (21) simplifies considerably for a flat plate at zero angle of attack for which $V(Z_o)=V(X_w)=U$ and $\alpha=\lambda=0$, so using Eq. (14) gives

(22)

$$\left(F_x + iF_y\right)_u = 2i\rho\gamma_o U\,\mathrm{Re}\left(\frac{a^2}{z_o^2-a^2}\right)+i\rho U\int_{-\infty}^{t}\mu(\tau)\left(\frac{x_w^2+a^2}{x_w^2-a^2}\right)d\tau.$$

Expanding both terms using partial fractions gives

(23)

$$\left(F_x + iF_y\right)_u = i\rho\gamma_o U\,\mathrm{Re}\left(\frac{a}{z_o-a}-\frac{a}{z_o+a}\right)+\frac{i\rho U}{2}\int_{-\infty}^{t}\mu(\tau)\left(\frac{x_w+a}{x_w-a}+\frac{x_w-a}{x_w+a}\right)d\tau.$$

This shows that the vortex induces a pulse at $z_o=-a$ and $z_o=a$ but, by using Eq. (6), we see that the term dependent on $(z_o-a)^{-1}$ exactly cancels the singularity of the convolution integral that occurs when $x_w=a$. Combining Eq. (6) and Eq. (23) gives

(24)

$$\left(F_x + iF_y\right) = -i\rho\gamma_o aU\,\mathrm{Re}\left\{\frac{1}{z_o+a}\right\}+\frac{i\rho U}{2}\int_{-\infty}^{t}\mu(\tau)\left(\frac{x_w-a}{x_w+a}\right)d\tau.$$

The first term represents the leading edge pulse and the second the contribution from the wake. It will be shown in the appendix that Eq. (24) reduces to the result that would have been obtained if the analysis had been carried out in the frequency domain using Sears function.

3. Discussion

3.1 Results for a flat plate

To verify the results given above we will first consider the case of a flat plate at zero angle of attack in a uniform flow for which the unsteady lift can be calculated using Sears function. Using Eq. (24) the unsteady loading can be split into two parts: the first is the

leading edge pulse given by the first term in (24) and the second is the wake pulse given by the second term in Eq. (24). The leading edge pulse is relatively simple to evaluate from the potential mean flow, but the wake pulse requires the evaluation of a convolution integral which is more involved. It is shown in the appendix how this can be solved using Fourier Transforms and an analytical solution is derived which reduces to the same result
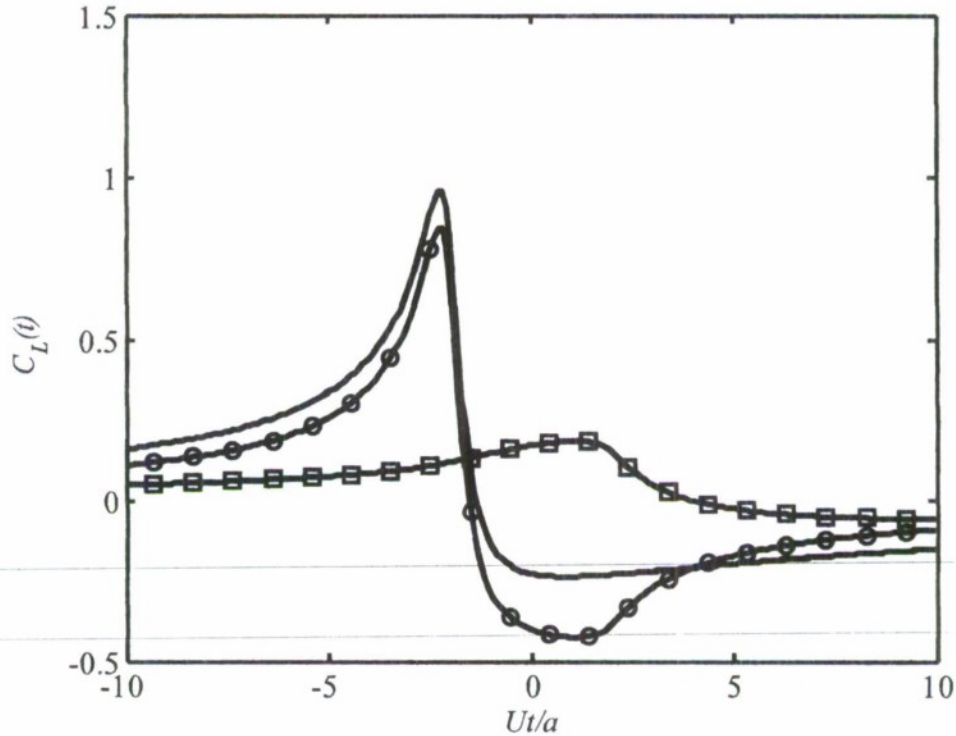

Fig. 1: The unsteady lift coefficient $C_L(t)=L(t)/\rho U \gamma_0$ for a vortex passing at a distance $4a/10$ above a flat plate. —o— leading edge pulse, —□— pulse induced by the wake, — sum of the two pulses.

as would have been obtained by utilizing Sears function. The relative magnitude of the leading edge and wake pulses is illustrated in Fig. 1, which shows the unsteady lift $L(t)=F_y(t)$ for a vortex passing a distance $4a/10$ above a flat plate. The leading edge pulse clearly dominates and the wake pulse is only important as the vortex passes the mid chord point at time $Ut/a=0$. The vortex passes the trailing edge at time $Ut/a=2$ and both the leading edge and wake pulses show a sharp change in slope at this point. However the net effect is negligible as shown by the sum of the two pulses. The overall signature is dominated by the leading edge interaction, and the sharpness of the pulse depends on the distance of the vortex from the airfoil.

The spectra of the time histories $\tilde{L}(\omega)$ shown in Fig. 1 have been normalized by the upwash spectrum of the gust $\tilde{v}(\omega)$ (see Eq. (A5))and compared to Sears function in Fig.

11

2 as a function of the non dimensional frequency $\sigma=2\omega a/U$. The plots show the non dimensional lift response function $S_L(\omega) = |\tilde{L}(\omega)/4\pi\rho a U\tilde{v}(\omega)|$. At non dimensional frequencies $\sigma>10$ the spectrum of the leading edge pulse is identical to Sears function, but at lower frequencies it exhibits an oscillatory behavior and asymptotes to 0.5 for $\sigma\ll1$. The magnitude of the contribution from the wake is also shown and this is clearly
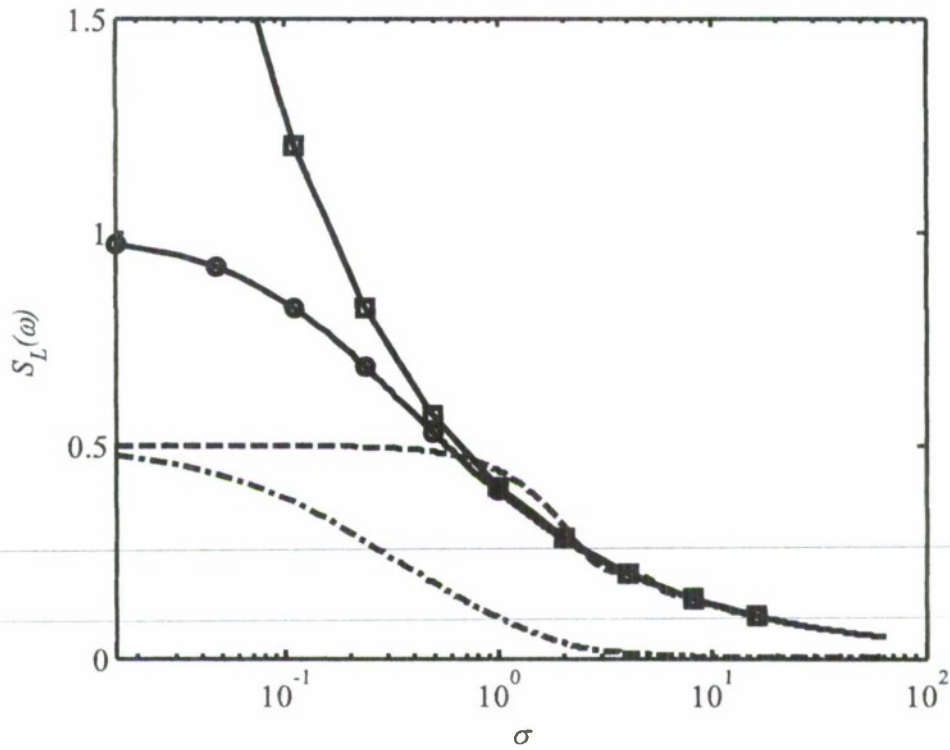

Fig. 2: Lift response function magnitude $S_L(\omega) = |\tilde{L}(\omega)/4\pi\rho a U\tilde{v}(\omega)|$ as a function of reduced frequency σ for a flat plate showing the contribution of the wake (— • —) and the leading edge (dashed line — —). The total unsteady lift (the Sears function) is presented both as the theoretical calculation (o) and as the sum of the leading edge and wake response (solid line). Also shown is the high frequency approximation for Sears function (.—□—)

only important at low frequencies ($\sigma<3$). The sum of the leading edge contribution and the wake contribution exactly matches the Sears function as shown. At low frequencies the leading edge and wake contributions are in phase and add to give a level which asymptotes to one. At non dimensional frequencies $\sigma\sim1$ the two terms are out of phase and the leading edge contribution is reduced by the wake contribution. It is also interesting to consider the high frequency approximation to the Sears function whose magnitude is given by $1/\sqrt{2\pi\sigma}$. This is a good approximation at non-dimensional frequencies $\sigma>1$ but tends to infinity at low frequencies. In the frequency range $1<\sigma<10$ it is a better approximation than the leading edge response in isolation.

The evaluation of the convolution integral in Eq. (24) can also be carried out numerically using Fast Fourier Transforms, as shown in the appendix. While this is not necessary for the flat plate, it will be required for an airfoil of finite thickness or at an angle of attack and so the accuracy of the numerical method needs to be established. Fig. 3 shows a comparison of the wake pulse calculated numerically and theoretically as a function of frequency. It is seen that, apart from the lowest frequency bin, the error in the numerical method is very small and should give accurate results when applied to different configurations.
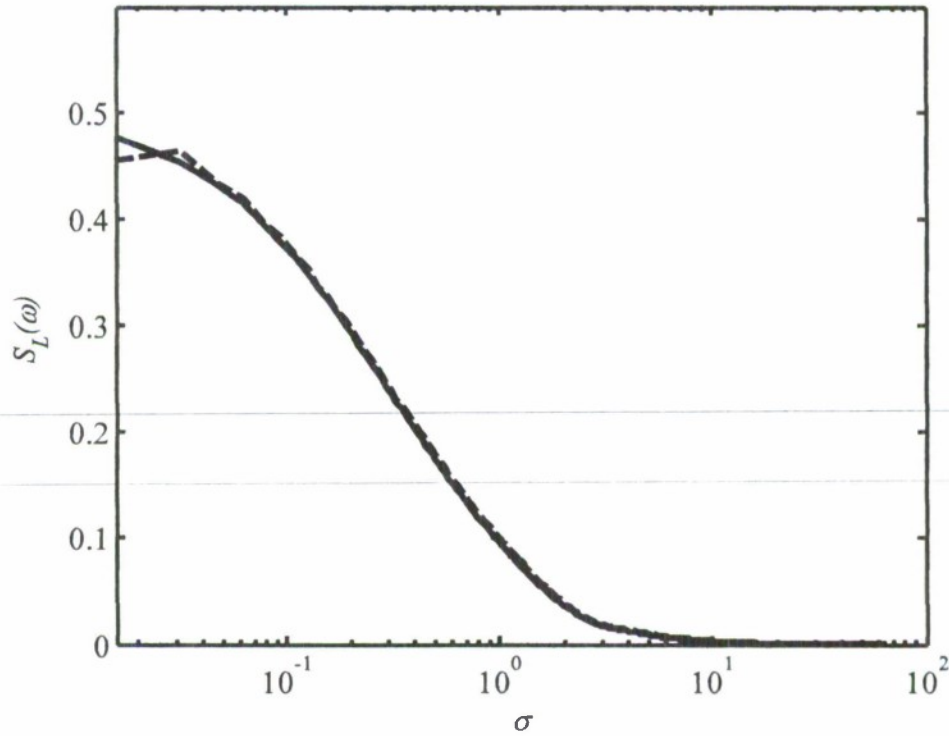

Fig. 3: Comparison between the lift response function $S_L(\omega) = |\tilde{L}(\omega)/4\pi\rho a U \tilde{v}(\omega)|$ induced by the wake of a flat plate calculated numerically (dashed line) and using the theoretical formulation (solid line) given in the appendix. Note that errors are only significant at the lowest reduced frequencies. Number of points used in the transform is 8196 and the reduced frequency resolution is 0.0157.

3.2 The effect of thickness and angle of attack

To demonstrate the effects of thickness and angle of attack on the unsteady loading Fig. 4 shows a calculation (using the approach described in the appendix) for a vortex passing an airfoil with a thickness to chord ratio of 0.15, at three different angles of attack. The results are presented as lift and drag components where the lift is given as the unsteady loading normal to the direction of the flow, $L=imag((F_X+iF_Y)exp(-i\alpha))$ and the drag is in

the direction of the flow and given by $D=real((F_X+iF_Y)exp(-i\alpha))$. The vortex is initiated at a point on a streamline which, at upstream infinity, would have been a distance equal
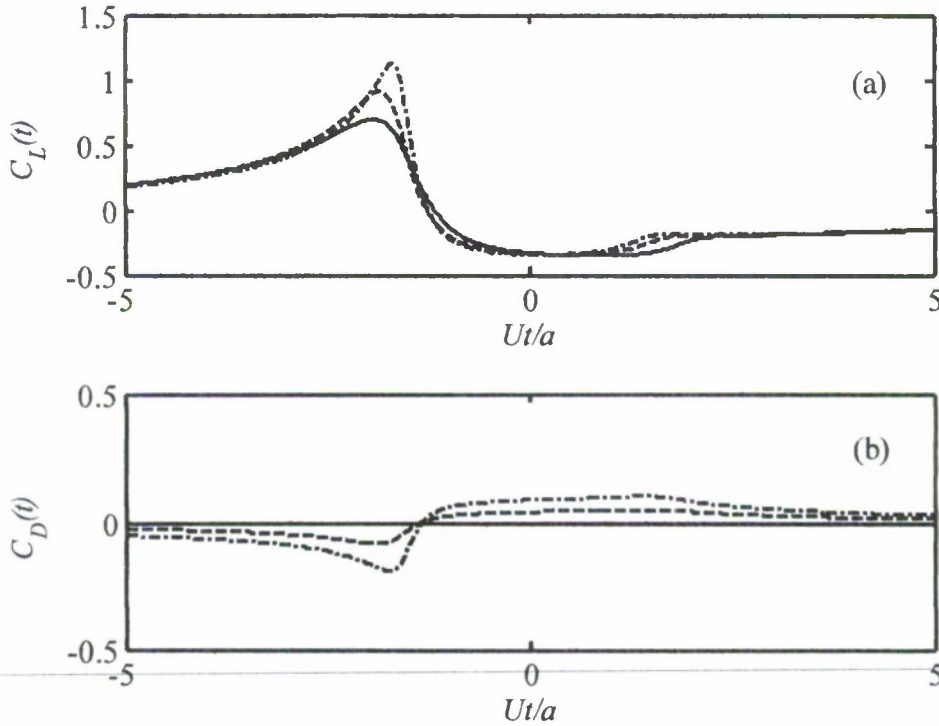

Fig. 4: (a) The unsteady lift coefficient $C_L(t)=L(t)/\rho U\gamma_o$ and (b) unsteady drag coefficient $C_D(t)=D(t)/\rho U\gamma_o$ for a vortex initiated at 10% of the chord above the stagnation streamline for airfoils at different angles of attack. Airfoil thickness to chord ratio is 0.15. Angle of attack: —— 0 deg , — — 5 deg, — • — 10 deg.

to 10% of the chord above the stagnation streamline. The initiation point of the vortex should therefore be independent of the angle attack and thickness of the airfoil. Fig. 4 shows that the unsteady lift can be represented by a pulse which peaks as the vortex passes the leading edge, but, as in the case of the flat plate, there is no apparent trailing edge pulse. The amplitude of the leading edge pulse increases with angle of attack. In contrast the unsteady drag exhibits a leading edge pulse which is negative causing leading edge suction which increases with angle of attack. When the vortex has passed the leading edge the drag is positive and decays slowly to zero as the vortex progresses.

3.3 Response to a step function upwash gust

An alternative gust type is a step upwash gust which can be represented by a sheet of vorticity normal to the direction of the incident flow at upstream infinity. In a uniform mean flow, and assuming Rapid Distortion Theory, the gust convects without modifying

14

itself and represents a step change in upwash velocity. The step gust, while unrealizable in practice, is a reasonable model for a large lengthscale turbulent gust, and the unsteady
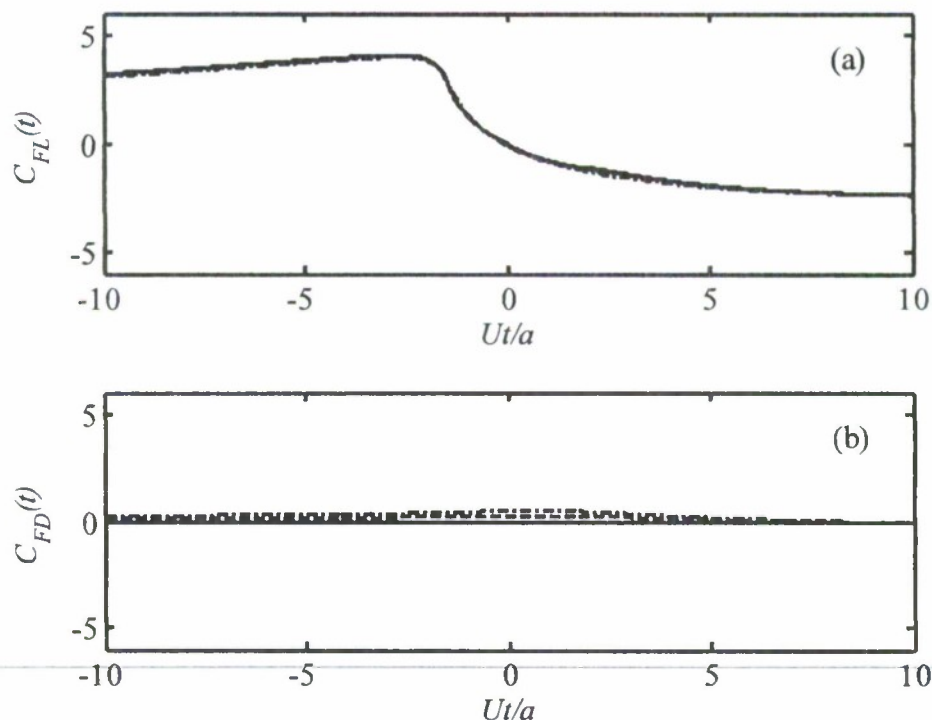

Fig. 5: The unsteady loading coefficients $C_{FL}(t)=F_L(t)/\rho U \Delta v a$ and $C_{FD}(t)=F_D(t)/\rho U \Delta v a$ for a step function incident on an airfoil at angles of attack of 0 (solid line), 4 (dashed line) and 8 degs(dashed dot line). Airfoil thickness to chord ratio is 0.15. The direction of the force component F_L (shown in (a)) is rotated forward from the lift force direction by an angle equal to the angle of attack, and the force F_D is normal to F_L.

loading caused by a step gust will be indicative of the loading from the low wavenumber components of the turbulence spectrum. To model a step gust the vortex sheet is specified by the superposition of elemental vortices of strength $\gamma_o = \Delta v \Delta h$ separated by the distance Δh where Δv is the magnitude of the velocity jump across the step gust. To avoid numerical errors we need to ensure that a vortex is not placed on the stagnation streamline (see section 3.5 for numerical details).

The unsteady loading from a step gust can be calculated using the approach described above by summing the contributions from each elemental vortex and the results are presented in Fig. 5. In this case we expect (from Howe [6]) that the effect of angle of attack on the unsteady loading will be to rotate the loading vector forward by an angle equal to the angle of attack. To illustrate this effect the results presented in Fig. 5 are for the forces relative to the direction of the loading suggested by Howe, which is rotated forward by 2α from the direction of the chord. This gives the forces

15

$F_L = imag((F_X + iF_Y)exp(-2i\alpha))$ and $F_D = real((F_X + iF_Y)exp(-2i\alpha))$. If Howe's theory for a flat plate applies to an airfoil of finite thickness then the pulses shown in Fig. 5 should be independent of angle of attack, which is clearly the case for F_L. The force F_D shows a small increase with angle of attack but this is smoothly varying and relatively insignificant.

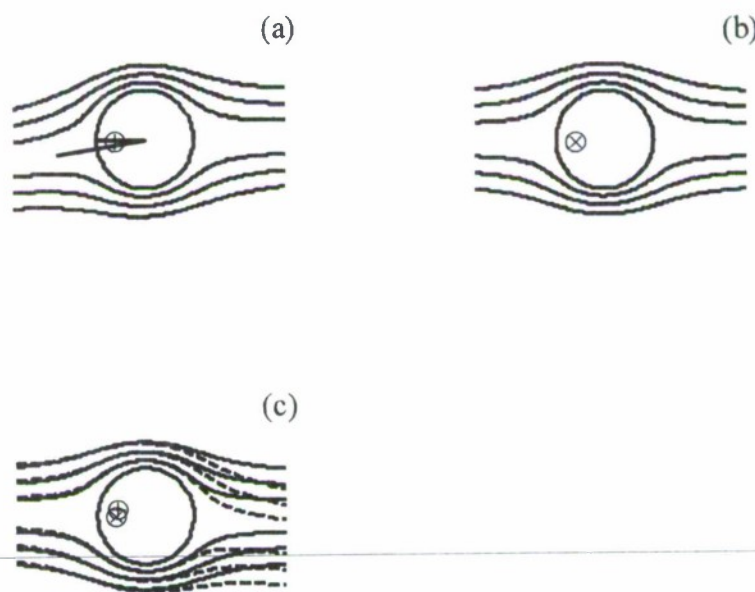(a)   (b)

(c)

Fig. 6: Vortex trajectories in the circle plane showing that they are almost identical in the leading edge region for all angles of attack if the leading edge stagnation points are aligned. (a) vortex trajectories at 5deg angle of attack, (b) vortex trajectories at 0deg angle of attack, (c) Overlay of (b) onto (a) rotated clockwise by twice the angle of attack. (x) location of singular pint for zero angle of attack, (+)location of singular pint for 5 deg angle of attack

An explanation of the effects which are taking place as the airfoil thickness and angle of attack are changed is given by Fig. 6 which shows the flow about the airfoil in the circle plane. For a step gust a vortex will be convected along each of the streamlines shown in the figure and the amplitude of the leading edge pulse will depend on the distance of the vortices from the leading edge singular point which is located at $z = -a + 2\lambda$, and shown in the figure by the small circle. The effect of increasing the airfoil thickness is to move the singular point to a smaller radius, which will cause the loading pulse to be smoothed. Fig. 6(a) shows the flow at an angle of attack, and Fig. 6(b) shows the flow at zero angle of attack. In Fig. 6(c) the stream lines from 6(a) have been rotated clockwise by an angle equal to twice the angle of attack, and overlaid onto the zero angle

of attack case. The trajectories of the vortices are now almost identical. For the angle of attack case the vortices on the upper (suction) side of the airfoil pass closer to the leading edge singularity than the vortices on the lower (pressure) side of the airfoil. For a blade vortex interaction, as considered in the previous section, the proximity of the vortex to the leading edge singularity is the dominant feature that affects the magnitude and shape of the unsteady loading pulse. When the blade is at a positive angle of attack a vortex passing above the blade will always cause a larger unsteady loading pulse than a vortex passing below the airfoil. In contrast, for a step gust Fig. 5 indicates that the increased contribution from the vortices on the upper side is offset by the reduced contribution of the vortices on the lower side, and this conclusion is only weakly affected by the airfoil thickness.

3.4 Lift sensitivity diagrams

Fig. 7 shows contours of the unsteady lift as a function of the physical coordinates of the vortex as it convects past the airfoil for three different thickness to chord ratios at an angle of attack of 8 deg. These pictures reveal the sensitivity of the airfoil to a vortical disturbance as a function of the position of that disturbance in the flow field. For the thickness to chord ratio of 0.15 the sensitivity reaches a maximum just ahead of the leading edge, at a point displaced about 3% chord ahead of the leading edge on the chord line. Closer to the airfoil surface the sensitivity drops considerably as the airfoil surface is approached. The plots for the thinnest and thickest airfoil show that the location of the maximum lift sensitivity moves away from the surface as the thickness increases. Unsteady drag sensitivity can be plotted in the same way (Glegg, Devenport and Staubs [19]) and are typically one quarter of those of the unsteady lift. The trailing edge does have a noticeable influence, locally distorting both the lift and drag contours (not shown).

The same results are shown in Fig. 8 in terms of the initial vortex position Ψ/Ua and time Ut/a which are identical to the non dimensional drift coordinates of the flow (where Ψ is the mean flow stream function). These pictures show quite explicitly the effect of flow distortion on the response. In physical coordinates the point of greatest sensitivity appears ahead of the airfoil leading edge, on the suction side of the stagnation streamline. The same maximum appears at positive values of Ψ in drift coordinates. Asymmetry is also introduced because of the way the distortion affects the relative timing of events on the upper and lower surfaces. Since the travel time of fluid passing to the suction side of the airfoil is significantly shorter than that of fluid passing to the pressure side, events occurring at the same physical position are dislocated in time across the streamline $\Psi=0$. A good example is the response features associated with the trailing edge, that are significantly advanced on the suction side and retarded on the pressure side and thus are not phase aligned.

Fig. 9 shows the same the lift sensitivity as a function of location in the circle plane for the different airfoil thicknesses. These also show how the peak lift sensitivity moves away from the surface as the thickness is increased.
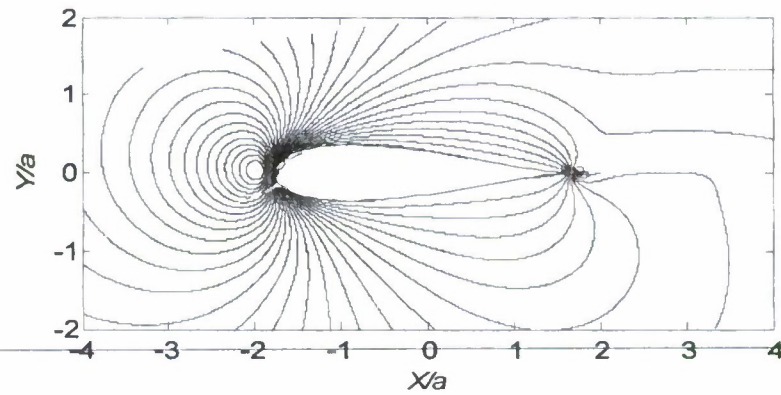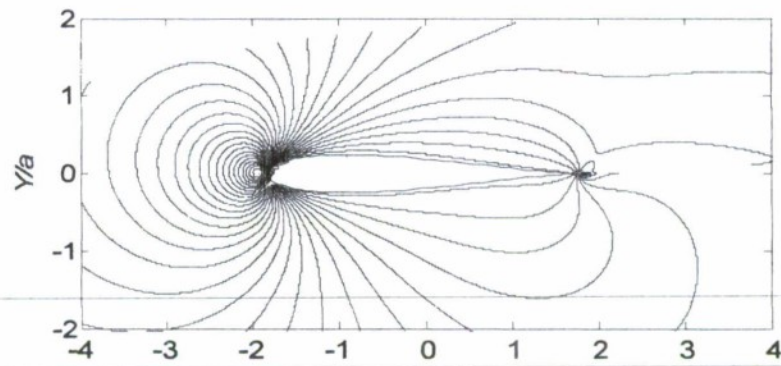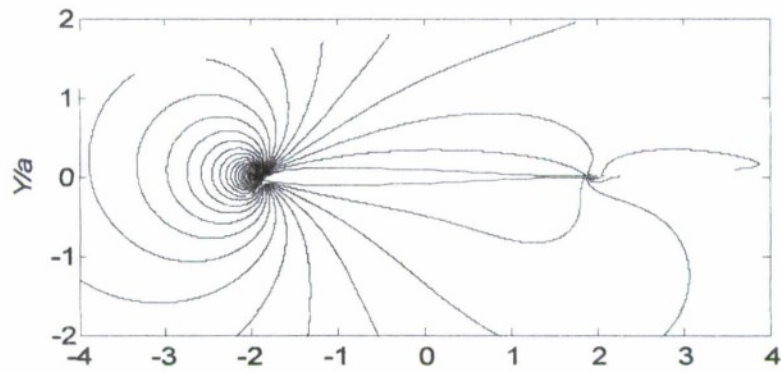
Fig. 7: Unsteady Lift sensitivity plots for airfoils of thickness to chord ratios of 0.06, 0.15 and 0.24. Contours show the magnitude of the unsteady lift for each vortex location in the physical plane ($X/a, Y/a$).
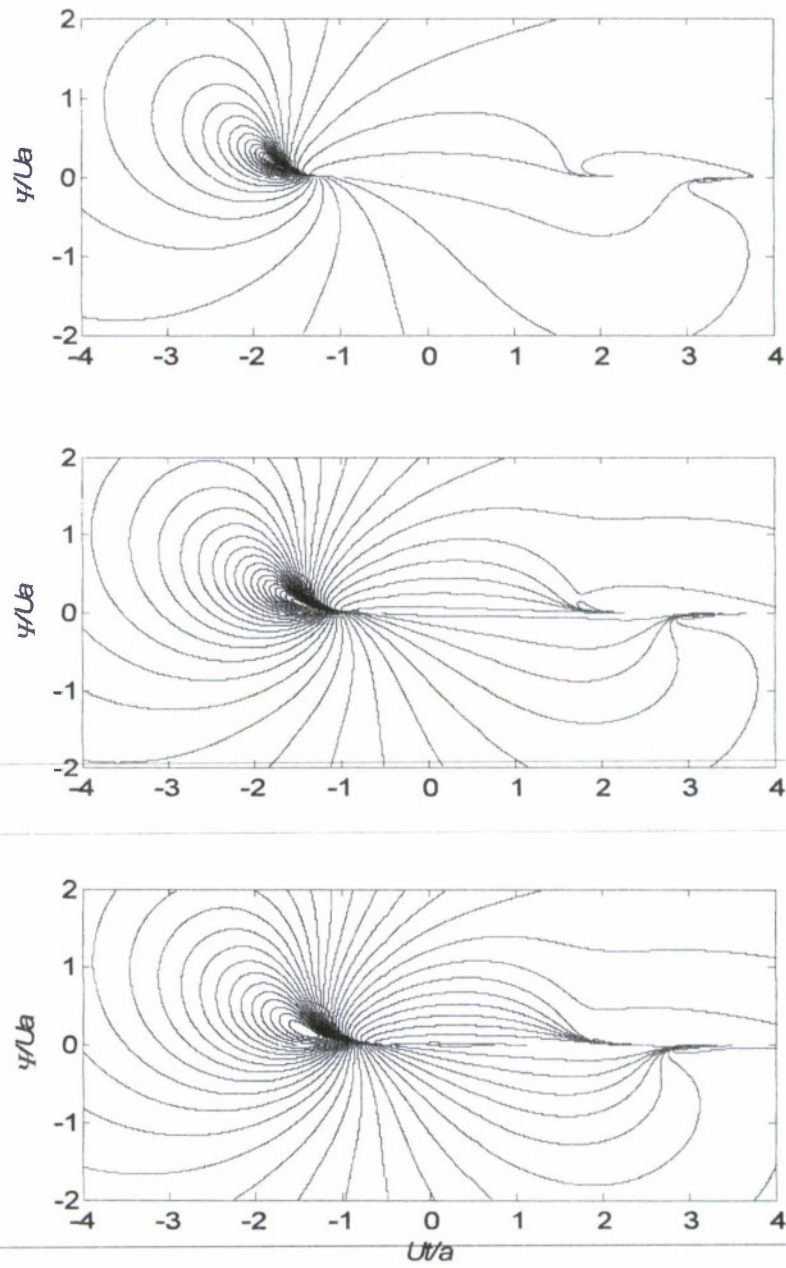
18

Fig. 8: Unsteady Lift sensitivity plots for airfoils of thickness to chord ratios of 0.06, 0.15 and 0.24. Contours show the magnitude of the unsteady lift for each vortex location in drift coordinates (Ut/a, Ψ/Ua).
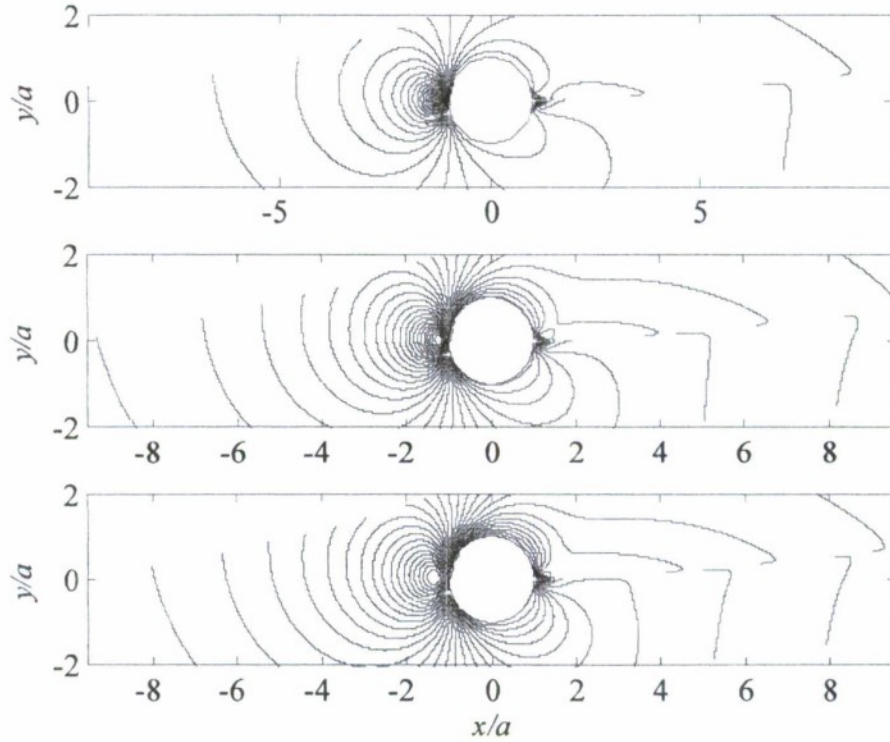
19

Fig. 9: Unsteady Lift sensitivity plots for airfoils of thickness to chord ratios of 0.06, 0.15 and 0.24. Contours show the magnitude of the unsteady lift for each vortex location in the circle plane $(x/a, y/a)$.

Further insight into the sensitivity close to the leading edge is obtained by considering the leading edge pulse in more detail. Using Eq. (15) in Eq. (13) and retaining only those terms which are singular at $z_o = -a + 2\lambda$ gives

(25)

$$\left(F_x + iF_y\right)_v \approx \frac{-i\rho\gamma_o}{2}\left\{\frac{a_c V(Z_o)}{z_c + a_c} + \left(\left(\frac{az_c}{a_c z_o}\right)^2 \left(\frac{a_c V(Z_o)}{z_c + a_c}\right)\right)^*\right\} + \ldots\ldots,$$

where $z_c = z_o - \lambda$ and $a_c = a - \lambda$. The unsteady lift from the leading edge pulse is then obtained by multiplying Eq. (25) by $-i\exp(-i\alpha)$ and evaluating the real part so

(26)

$$L_{LE} = -\frac{\rho\gamma_o}{2}\operatorname{Re}\left[\left(1 + \left(\frac{az_c e^{i\alpha}}{a_c z_o}\right)^2\right)\left(\frac{a_c V(Z_o)e^{-i\alpha}}{z_c + a_c}\right)\right].$$

The velocity is given by

(27)

$$V(Z_o) = \left(\frac{(1 - a/z_o)(1 + ae^{2i\alpha}/z_o)Ue^{-i\alpha}}{1 - (a_c/z_c)^2}\right)^*.$$

20

In the leading edge region the function L_{LE} is quite complicated with a second order pole at $z_c=-a_c$ and a zero at the stagnation point $z_o=-a\exp(-2i\alpha)$. The influence of the singularity will dominate the lift sensitivity close to the leading edge, and so we can assume that when $z_o\sim-a$ we can approximate $az_c=a_cz_o$, so

(28)

$$L_{LE} \approx -\frac{\rho\gamma_oU_\infty}{2}\mathrm{Re}\left[\left(1+e^{2i\alpha}\right)\left(\frac{a_c^3(z_o+ae^{2i\alpha})^*}{a^2|z_c+a_c|^2}\right)\right].$$

The largest values of this function occur when the vortex lies on the real axis and if this function is evaluated for $z_o=x_o$ we find

(29)

$$L_{LE} \approx -\frac{\rho\gamma_oU_\infty}{2}\left(\frac{a_c^3(x_o+a)(1+\cos(2\alpha)))}{a^2(x_o+a-2\lambda)^2}\right).$$

The function has a zero at $x_o=-a$ and by differentiating with respect to x_o we find it also has a maximum at $x_o=-a-2\lambda$, which is upstream of the leading edge and dominates the contour plots in Figs. 7,8 and 9.

The interesting feature about the lift sensitivity plots is that they show the unsteady lift peaks as the vortex passes the leading edge, but if the vortex is too close to the leading edge the response is reduced. The maximum level occurs when the vortex passes at a distance 2λ in front of the leading edge in the circle plane. The location of this maximum moves upstream and its magnitude is reduced as the thickness is increased.

3.5 Unsteady lift spectra

The spectral characteristics of the unsteady lift will be illustrated by taking the Fourier transform of the unsteady loading time history for the step function gust used in section 3.3. The gust is generated by an array of equally spaced point vortices along a line which is initiated at 90 deg to the stagnation streamline at a point which is 30 chord lengths upstream of the center of the airfoil. The vortices are separated by $4a/100$ and the minimum displacement from the stagnation streamline is $4a/200$ (it is shown in [19] that the spectra converge when the minimum displacement of the vortex is less than $4a/100$). To generate a step function the length of the vortex array should be infinite, but for the purpose of numerical calculations it is limited to $40a$. The resulting upwash gust is plotted as a function of Ut/a in Fig. 10, and is seen to be a rather poor model of a step function, but it does include a step discontinuity at $t=0$. The spectrum of this gust is shown in Fig. 11 and it is seen to have a slope of $1/\omega^2$ at high frequencies. Some care must be exercised when numerically evaluating spectra for time histories such as those
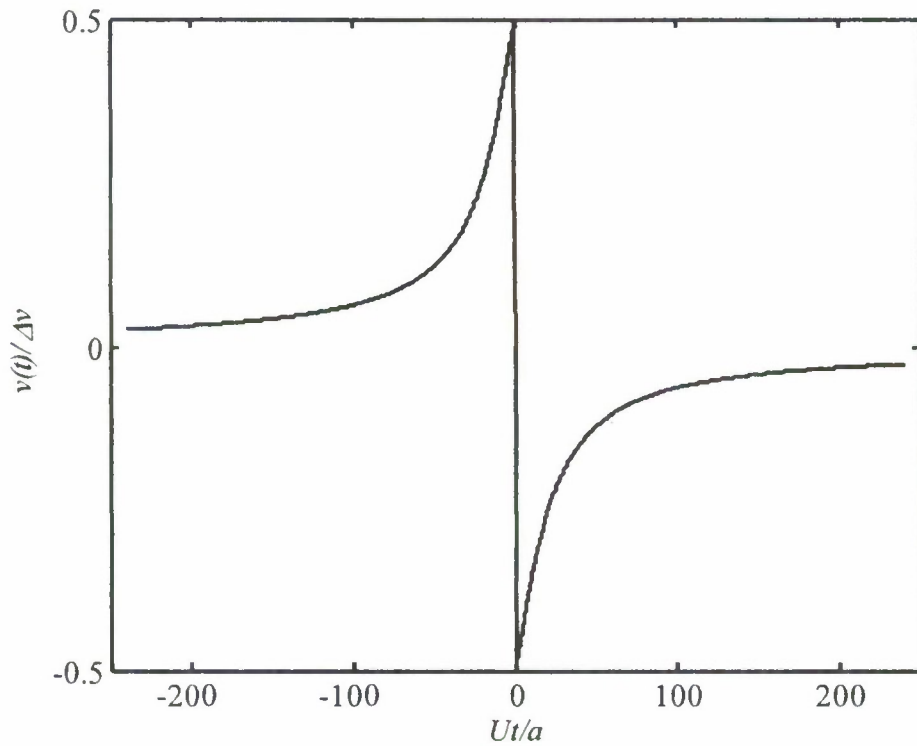
Figure 10: The upwash gust velocity for a vortex sheet of unit strength, which is used in the calculations of lift spectra. The upwash $v(t)/\Delta v$ is plotted as a function of non dimensional time Ut/a (Note airfoil chord is ~$4a$)

illustrated in Fig. 10. The spectra were calculated with 32784 points for signatures between $-UT/a<Ut/a<UT/a$ with UT/a=240 and using a window function defined by $\cos^2(\pi t/T)$. The time history was also folded so that the discrete Fourier Transform was applied over $0<t<2T$ to a periodic time sequence made up of repeated pulses.

Fig. 12 shows the spectrum of the total unsteady loading $\tilde{F}_T^2(\omega)=|\tilde{F}_L(\omega)|^2+|\tilde{F}_D(\omega)|^2$ for the airfoil with a thickness to chord ratio of 0.001 at 0,4 and 8 degrees angle of attack. Also plotted on this graph is the response obtained by multiplying the gust spectrum by Sears function. Fig. 12 shows that the spectra are independent of angle of attack, confirming our previous conclusions. The only exception is the 8 deg angle of attack case which deviates from the other results at reduced frequencies above 10, showing a slight decrease in level. Increasing the thickness reduces the rate of change in the gust time history and the high frequency loading response function is reduced as illustrated in Fig. 13, for an airfoil with a thickness to chord ratio of 0.15. Comparing Figs. 12 and 13 shows a reduction in level due to thickness, but the effects of angle of attack remain the same in each case.
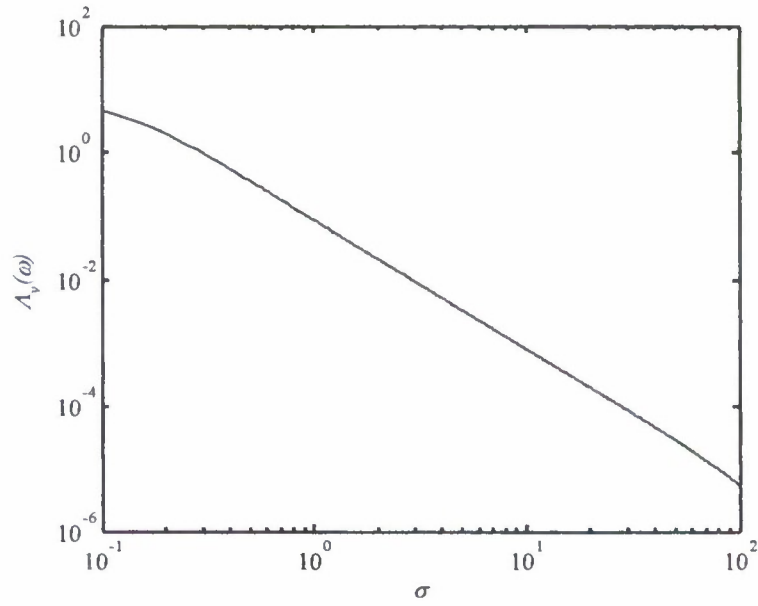
Figure 11: The spectrum of the gust $\Lambda_v(\omega) = |\, \tilde{v}(\omega)U \,/\, a\Delta v\,|^2$ used for the calculation of lift spectra as a function of reduced frequency σ.

Fig. 12: Unsteady loading spectra $\Lambda(\omega) = |\, \tilde{F}_T(\omega) \,/\, \rho a^2 \Delta v\,|^2$ as a function of reduced frequency σ for an airfoil with a thickness to chord ratio of 0.001 at angles of attack of 0 deg, 4 deg and 8 deg. — • — Spectrum based on Sears function. — Spectra for different angles of attack.
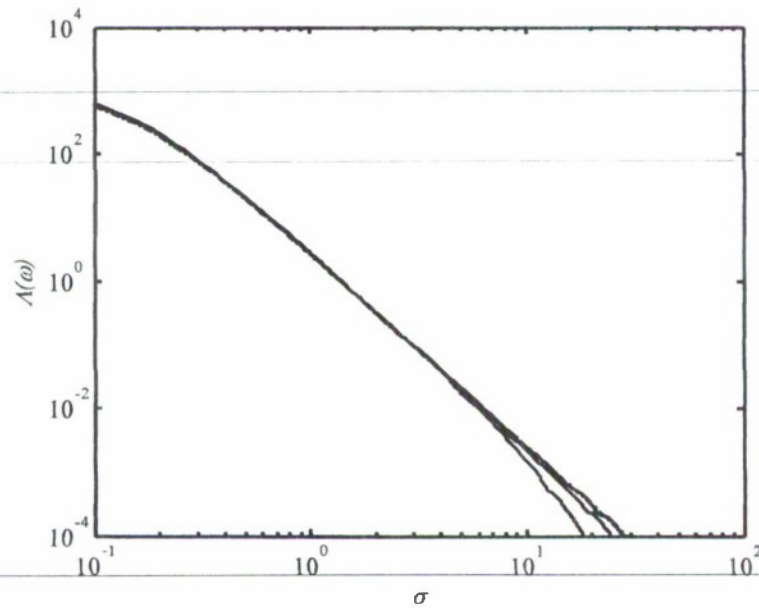
Fig. 13: Unsteady loading spectra $\Lambda(\omega) = |\widetilde{F}_T(\omega)/\rho a^2 \Delta v|^2$ as a function of reduced frequency σ for an airfoil with a thickness to chord ratio of 0.15 at angles of attack of 0 deg, 4 deg and 8 deg. ━ • ━ Spectrum based on Sears function. ━ Spectra for different angles of attack.
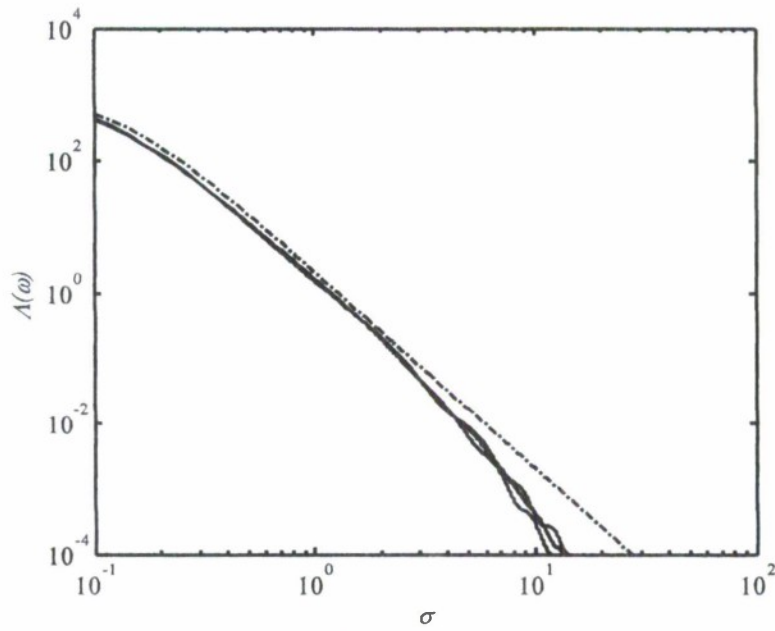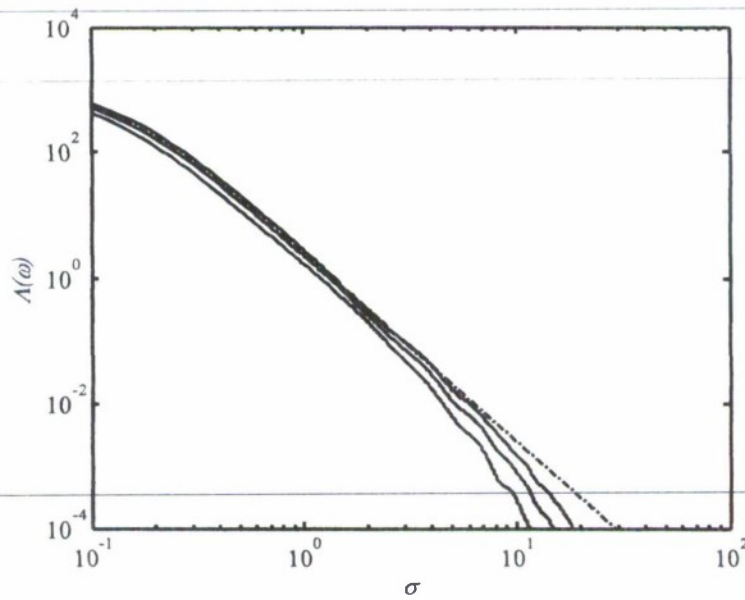

Fig. 14: Unsteady loading spectra $\Lambda(\omega) = |\widetilde{F}_T(\omega)/\rho a^2 \Delta v|^2$ as a function of reduced frequency σ for airfoils with thickness to chord ratios of 0.001, 0.06, and 0.15 at an angle of attack of 8 degs. ━ • ━ Spectrum based on Sears function. ━ Spectra for different angles of thickness airfoils. Lower levels are thicker airfoils.

24

Fig. 14 shows the effects of thickness to chord ratio for an airfoil at an angle of attack of 8 deg. In all cases the amplitude of the response decreases with increased thickness especially at high frequencies. It is interesting to contrast this result with its time history shown in Fig. 15. These show that the signature for the thinnest airfoil has the sharpest change of slope as the gust passes the leading edge, and so we would expect thickness to reduce the spectral level at high frequencies.

Finally we note that the numerical results presented in this paper based on the analytical approach given in section 2, have been confirmed using a panel method (Glegg, Devenport and Staubs[19]).

4. Conclusions

The unsteady loading on a two dimensional airfoil in an incompressible flow has been evaluated for an airfoil of arbitrary thickness and angle of attack, without applying the assumptions of thin airfoil theory. It has been shown that the unsteady loading is dominated by the leading edge pulse and the application of the Kutta condition cancels
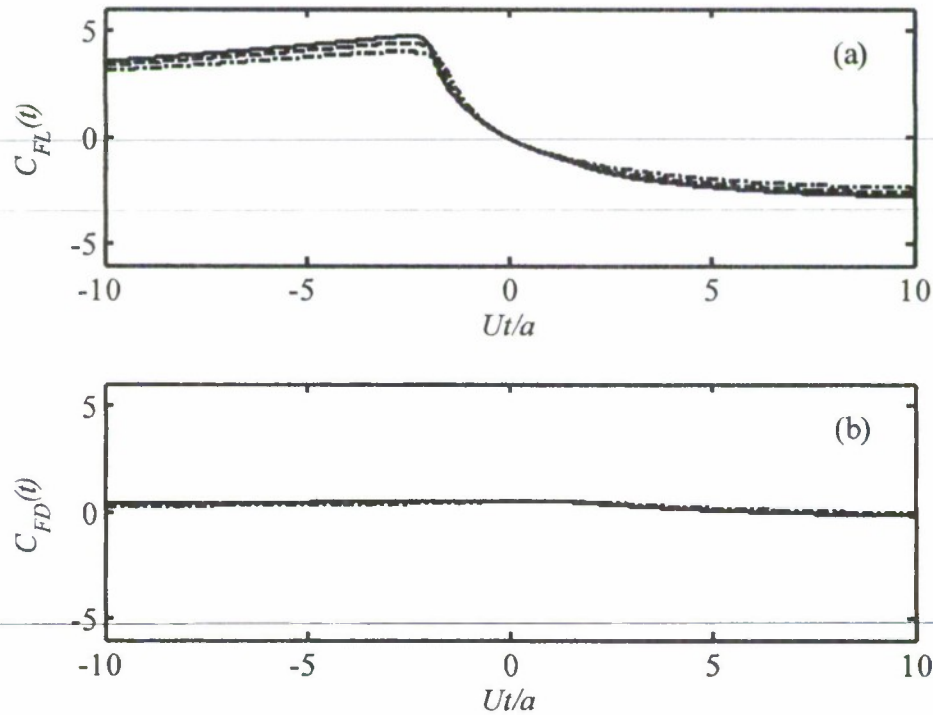

Fig. 15: The unsteady loading coefficients $C_{FL}(t)=F_L(t)/\rho U \Delta v a$ and $C_{FD}(t)=F_D(t)/\rho U \Delta v a$ for a step function incident on an airfoil (see figure 5) for airfoils of thickness to chord ratios of 0.001(solid line), 0.06 (dashed line) and 0.15 (dashed dot line) at 8 deg angle of attack.

the pulse generated as the gust passes the trailing edge, extending previously known results for flat plates to airfoils of finite thickness and angle of attack.

For a blade vortex interaction the unsteady loading depends on the passage of the vortex relative to the leading edge singularity in the circle plane. As the airfoil thickness is increased this singularity moves to a smaller radius, smoothing the pulse. When the airfoil is at an angle of attack the stagnation point is moved relative to the singularity and the unsteady loading pulse depends on whether the vortex passes the airfoil on the suction or pressure side. If it passes on the pressure side it will always be further from the leading edge singularity than if it passes on the suction side, and so the unsteady loading pulse is reduced.

The characteristics of the unsteady loading are quite different for a step upwash gust, which is more representative of a large scale turbulent flow than a single blade vortex interaction. For a step gust the magnitude of the unsteady loading time history is almost unaltered by changes in angle of attack α but the direction of action of the force is rotated forward so that it makes an angle α with the lift direction. This extends the result obtained by Howe [6] for a flat plate in turbulent flow to an airfoil of arbitrary thickness subjected to a symmetric gust. However spectral analysis of the gust shows that the high frequency blade response is reduced as the thickness of the airfoil is increased.

One of the most important applications of this theory is to airfoils in a turbulent flow. To extend the analysis to include a turbulent inflow a full three dimensional calculation must be carried out and the effect of chopping of the vortex lines normal to the plane of the airfoil must be considered. In addition, the spanwise correlation length scale of the turbulence must be included. These issues are considered in [20].

Appendix A: Numerical Evaluation

The unsteady loading is given in Eq. (21) as the sum of the loading from the vortex motion, given by

$$ (A1) $$

$$ i\rho\gamma_o\left\{\frac{(a-\lambda)^2}{(z_o-\lambda)^2}\left(\frac{dz_o}{dt}\right)+\left(\frac{a^2}{z_o^2}\frac{dz_o}{dt}\right)^{\bullet}+V(Z_o)-Ue^{i\alpha}\right\}, $$

and the unsteady loading from the wake given by

$$ (A2) $$

$$ i\rho\int_{-\infty}^{t}\mu(\tau)V(X_w)\left(\left\{1+\frac{a^2}{x_w^2}\right\}\frac{(x_w-\lambda)^2}{(x_w-\lambda)^2-(a-\lambda)^2}\right)d\tau. $$

For a vortex in a potential mean flow specified by Eq. (2) it is relatively straight forward to determine the vortex position $z_o(t)$ and velocity dz_o/dt and hence evaluate (A1) to obtain the time history of the unsteady loading due to vortex motion. For the wake induced load given by (A2) the main difficulty is caused by the complexity of the

integrand in the convolution integral. To obtain a solution we first assume that the convection velocity of the vorticity in the wake is equal to the mean flow velocity at the trailing edge so $V(X_w)=V_{TE}=(1-\lambda/a)U\cos\alpha$. Then using Eq. (1) we can define the location of the vorticity in the wake as

$$(A3)$$

$$x_w(t,\tau) = \lambda + X_W(t,\tau)/2 + \sqrt{(X_W(t,\tau)/2)^2 - (a-\lambda)^2} \qquad X_W(t,\tau) = 2(a-\lambda) + (t-\tau)V_{TE}$$

The integral in Eq. (A2) may then be defined as

$$(A4)$$

$$i\rho \int_{-\infty}^{t} \mu(\tau)q(t-\tau)d\tau \qquad q(t) = V_{TE}\left(\left\{1 + \frac{a^2}{x_w^2}\right\}\frac{(x_w - \lambda)^2}{(x_w - \lambda)^2 - (a-\lambda)^2}\right)_{\tau=0}.$$

Using Fourier transforms with the notation convention

$$(A5)$$

$$\tilde{f}(\omega) = \frac{1}{2\pi} \int_{-\infty}^{\infty} f(t)e^{i\omega t}dt$$

gives Eq. (A4) as

$$(A6)$$

$$2\pi i\rho \int_{-\infty}^{\infty} \tilde{\mu}(\omega)\tilde{q}(\omega)e^{-i\omega t}d\omega.$$

To evaluate the vorticity distribution in the wake we use Eq. (5) with $v_v(t)=iw_v{}'(a,t)$ so

$$(A7)$$

$$\tilde{\mu}(\omega) = \frac{a\tilde{v}_v(\omega)}{\tilde{g}(\omega)} \qquad g(t) = \left(\frac{x_w + a}{x_w - a}\right)_{\tau=0}.$$

We can evaluate the Eq. (A6) numerically by combining it with Eq. (A7) and using discrete Fourier transforms based on the Fast Fourier Transforms algorithm. However some care has to be used in this numerical calculation because both $q(t)$ and $g(t)$ have a singularity of order $t^{-1/2}$ at $t=0$. Accurate numerical approximation of the integrals was achieved by ensuring that the numerical series representing $q(t),g(t)$ and $v_v(t)$ were the same length, used the same time step and satisfied the causality condition. The discrete of the time histories were therefore chosen as

$$v_n = v_v(n\Delta t - T) \quad g_n = \begin{cases} 0 & n\Delta t < T \\ g(n\Delta t - T) & n\Delta t > T \end{cases} \quad q_n = \begin{cases} 0 & n\Delta t < T \\ q(n\Delta t - T) & n\Delta t > T \end{cases}$$

where $1 \le n \le N$ and the time histories are defined at equal intervals Δt. The number of points in the sequence is N and must be a power of 2, so choosing $T=(N+1)\Delta t/2$ ensures that $g(t)$ and $q(t)$ are not evaluated at $t=0$. Numerical evaluation of Eq. (A6) was then obtained using

$$(A8)$$

27

$$2\pi i\rho a\int_{-\infty}^{\infty}\frac{\tilde{v}_v(\omega)\tilde{q}(\omega)}{\tilde{g}(\omega)}e^{-i\omega t}d\omega=2\pi i\rho aDFT\left[\frac{IDFT[v_n]IDFT[q_n s_n]}{IDFT[g_n s_n]}\right]$$

where DFT and IDFT represent discrete forward and inverse Fourier transforms used so that their sign conventions are the same as used in Eq. (A5). A smoothing function s_n is required to prevent truncation errors at the end points of the integral and $s_n=\cos^2(\pi(n\Delta t-T)/2T)$ was found to be effective for this purpose.

Analytical solutions can be obtained for the special case of a flat plate at zero angle of attack. The vortex passes a distance h above the plate and is uniformly convected at the free stream velocity U. The Fourier transform of the wake vorticity is obtained (Howe [8]) as

(A9)

$$\tilde{\mu}(\omega)=\frac{2U\tilde{v}_v(a,\omega)e^{i\sigma}}{ia(H_o^{(1)}(\sigma)+iH_1^{(1)}(\sigma))}\qquad\tilde{v}_v(a,\omega)=\frac{a\gamma_o}{2\pi U}(J_o(\sigma)+iJ_1(\sigma))e^{-|\omega h|/U},$$

where $\sigma=2\omega a/U$ and J_n and $H_n^{(1)}$ represent Bessel and Hankel functions of the first kind of order n.

The spectrum of the unsteady lift $L(t)=F_y(t)$ can be obtained from Eq. (24) and is specified using Fourier transforms as

(A10)

$$\tilde{L}(\omega)=-\rho U(\gamma_o\tilde{I}^{(+)}(\omega)/2+2\pi\tilde{\mu}(\omega)\tilde{q}(\omega))$$

$$\tilde{I}^{(\pm)}(\omega)=\frac{1}{2\pi}\int_{-\infty}^{\infty}\left\{\frac{a}{(z_o\pm a)}+\frac{a}{(z_o^*\pm a)}\right\}e^{i\omega t}dt=\frac{-ae^{-|\omega|h/U}}{U}(J_o(\sigma)\mp iJ_1(\sigma))$$

$$\tilde{q}(\omega)=\frac{1}{4\pi}\int_0^{\infty}\left(\frac{x_w-a}{x_w+a}\right)e^{i\omega t}dt=\frac{-ia}{4U}\left\{[H_o^{(1)}(\sigma)-iH_1^{(1)}(\sigma)]e^{-i\sigma}\right\}$$

It may be shown that, by introducing Eq. (A7) and using the Wronskian of the Bessel functions, Eq. (A8) reduces to the lift spectrum which would have been obtained by using Sears function directly, with the upwash gust specified by the vortex as it is convected past the plate.

References

[1] Sears, W. R. Some aspects of non-stationary airfoil theory and its practical applications. *Journal of the Aeronautical Sciences* 8 (1941) 104-108

[2] Amiet, R., Sears, W. R. The aerodynamic noise of small-perturbation subsonic flows. *Journal of Fluid Mechanics* 44 (1970) 227-235

[3] Goldstein, M. E., Atassi, H. M. A complete second order theory for the unsteady flow about an airfoil due to a periodic gust. *Journal of Fluid Mechanics* 74 (1976) 741-765

[4] Atassi, H. M. The Sears problem for a lifting airfoil revisited new results. *Journal of Fluid Mechanics* 141 (1984) 109-122

[5] Howe, M. S. On unsteady surface forces, and sound produced by the normal

chopping of a rectilinear vortex. *Journal of Fluid Mechanics* 206 (1989) 131-153

[6] Howe, M.S.,Correlation of lift and thickness noise sources in vortex airfoil interactions, *Journal of Sound and Vibration*, 137 (1990) 1-7

[7] Howe, M.S., Unsteady lift and sound produced by an airfoil in a turbulent stream, *Journal of Fluids and Structures*, 15 (2001) 207-225

[8] Howe, M. S. The influence of vortex shedding on the generation of sound by convected turbulence. *Journal of Fluid Mechanics* 76 (1976) 711-740

[9] Howe, M. S. *Acoustics of Fluid Structure Interactions* Cambridge University Press, Cambridge, 1998

[10] Gersfeld, J., Leading edge noise from thick airfoils in turbulent flows, *Journal of the Acoustical Society of America* 116 (2004) 1416-1426

[11] Martinez, R. and Rudzinsky, J., Analytic evaluation of shape effects on blade vortex interactions, Cambridge Acoustical Associates Report U-2466-402.14, 1997.

[12] Grace S M, Unsteady Blade Response: The BVI Model vs. the Gust Model, *Proceedings of the 7th AIAA/CEAS Aeroacoustics Conference*, Maastricht, may 2001, AIAA paper no 2001-2209

[13] Lockard,D.P. and Morris, P.J. Radiated Noise from Airfoils in Realistic Mean Flows, *AIAA Journal*, 36 (2001) 907

[14] Acheson, D.J., *Elementary Fluid Dynamics*, Clarendon Press, Oxford, 1990

[15] Batchelor G K and Proudman, I, The effect or rapid distortion on a fluid in turbulent motion, *Quarterly Journal of Mechanics and Applied Mathematics*, 7 (1954) 83-103

[16] Hunt J C R, A theory of turbulent flow around two-dimensional bluff bodies, *Journal of Fluid Mechanics*, 61 (1973) 625-706

[17] Goldstein M E, Unsteady vortical and entropic distortions of potential flows around arbitrary obstacles, *Journal of Fluid Mechanics*, 89 (1978) 433-468

[18] Atassi, H.M. and Grzedzinski, J.,Unsteady disturbances of streaming motions around bodies, *Journal of. Fluid Mechanics*, 209 (1989) 385-403

[19] Glegg, S, Devenport W., and Staubs J., Leading Edge Noise *Proceedings of the 13th AIAA/CEAS Aeroacoustics Conference*, Cambridge, MA, May 2006 AIAA Paper no 2006-2424-345

[20] Glegg, S, Devenport W., and Staubs J., Sound radiation from three dimensional airfoils in a turbulent flow *Proceedings of the 46th AIAA Aerospace Sciences Conference*, Reno, NV, January 2008, AIAA Paper no 2008-0052

PART B: Sound Radiation from Three Dimensional Airfoils in a Turbulent Flow

1.0 Introduction

The broadband noise from fans in turbomachinery is often dominated by the effects of unsteady loading caused by the response of the blades to a turbulent inflow. This is referred to as leading edge noise. For example, this mechanism dominates broadband rotor stator interaction noise, and is also important for low speed fans. The prediction of leading edge noise in low speed fans is directly related to the unsteady loading on the fan blades, and so a clear understanding of how this is affected by airfoil thickness and angle of attack is important for the optimization of blade sections for low noise. In this paper we will consider the unsteady loading on fan blades and show how it may be predicted for blades of arbitrary shape using a boundary element method.

The use of boundary element methods to calculate unsteady loadings in the time domain is not new. There have been multiple studies that have considered this approach but they have focused on blade vortex interactions (Rockwell[1], Grace[2]). However when the unsteady inflow cannot be readily described by a compact vortex most authors have opted to use a frequency domain analysis in which the incident disturbance is specified by a harmonic gust (for example: Amiet[3], Atassi[4], Kerschen and Myers[5], Howe[6], Gerschfeld[7], Lockhard and Morris[8]). These studies have used both analytical and numerical methods to consider the effect of both thickness and angle of attack on the radiated noise but only those which can be reduced to relatively simple analytical expressions[3,6,7] have been extended to turbulent inflow gusts. A discussion of the differences between the use of a time domain method based on blade vortex interactions and analyses based on harmonic gusts is given by Grace[2], who concludes that boundary element methods have a number of advantages over harmonic gust approaches but that they are more difficult to apply to turbulent flows because of the problems of modeling the turbulent inflow with a set of discrete vortices. In this paper it will be shown how this problem can be overcome by re-formulating the boundary element method in terms of the stagnation enthalpy which can be defined as the rate of change of a velocity potential. Results will be given for the unsteady loading on blades of different cross section and at different angles of attack and the calculations will be compared to wind tunnel measurements of the radiated noise levels for a number of different airfoils.

2.0 Numerical Approach

Boundary element methods for problems in incompressible flow are usually (Katz and Plotkin[9]) based on the solution to Laplace's equation applied to the velocity potential. For unsteady flows the incident gust is specified by its vorticity and the Biot Savort law is used to give the gust velocity incident on the blade surface. The gust is convected using the solution to the vorticity equation, and can include non-linear interactions between the vorticity and the local unsteady flow. However for three dimensional gusts the stretching of the vorticity by the mean flow can lead to numerical issues close to the blade surface where the stretching and vortex strength amplification are large. To overcome these

issues we will re consider the boundary element method by starting with Crocco's form of the momentum equation

$$\frac{\partial v}{\partial t} + \nabla B + \omega \times v = 0 \tag{1}$$

where v represents the flow velocity, B the stagnation enthalpy and ω the vorticity. All variables are a function of time t and their position $\mathbf{x}$. It is convenient to relate the stagnation enthalpy to a velocity potential φ, and the local pressure p using

$$B = -\frac{\partial \varphi}{\partial t} \qquad\qquad \frac{\partial p}{\partial t} = \rho \frac{DB}{Dt} \tag{2}$$

Consequently if we can solve for the velocity potential φ on the surface of the blade we can use (2) to obtain the local surface pressure, the unsteady loading and the radiated noise. Taking the divergence of (1) for an incompressible flow gives

$$\nabla^2 \dot{\varphi} = \nabla.(\omega \times v) \tag{3}$$

A solution to this equation is obtained using a standard approach for a flow field in the presence of a stationary surface specified by the function $f(\mathbf{x})=0$, (with $f<0$ inside the surface), as

$$\dot{\varphi}(\mathbf{x})H(f) = \int_{V_e} (\omega \times v)_i \frac{\partial G}{\partial y_i} dV(\mathbf{y}) + \int_S \dot{\varphi}(\mathbf{y}) \frac{\partial G}{\partial y_i} n_i dS(\mathbf{y}) \tag{4}$$

where V_e is the volume exterior to the surface S on which $f=0$, and $G=1/(4\pi|\mathbf{x}-\mathbf{y}|)$ is the free field Greens function. On the left of the equation $H(f)$ represents the Heavyside function so for points inside the volume the left hand side of this equation is zero.

A boundary element method can be specified using, for example, the approaches given by Katz and Plotkin[9] to solve this equation. We have chosen to use collocation points inside the surface and specify rectangular panels on the surface of the airfoil. The panels are distributed according to the approach given by Katz and Plotkin[9] and equally distributed along the span. The panel strength, which defines the function $\dot{\varphi}$ on the surface, is assumed constant for each panel and varies in time as the source term, given by the volume integral in (4), evolves. The unsteady surface pressure is then obtained from equation (2) and integrated over the surface to obtain the rate of change of unsteady loading, which is integrated over time to obtain the time history of the unsteady lift.

To satisfy the Kutta condition vorticity must be shed from the trailing edge of the blade. This is modeled by discrete vortex elements for each spanwise trailing edge panel. The shed vorticity is introduced at a location which is a distance $\varepsilon V_{TE}\Delta t$ downstream of the

trailing edge where V_{TE} is the trailing edge velocity, Δt is the time step and ε is optimized to eliminate trailing edge pulses.

To apply this method to turbulent flow we need to consider the source term given by the volume integral in some detail. This depends on the Lamb vector $(\omega \times v)_i$ which simplifies considerably if Rapid Distortion Theory and a two dimensional potential mean flow are assumed. In this case the Lamb vector reduces to

$$(5)$$

$$\omega \times \mathbf{v} \approx \omega \times \mathbf{U} = (\omega.\hat{\mathbf{n}})U\hat{\mathbf{z}} + \omega_3 U\hat{\mathbf{n}}$$

where $\hat{\mathbf{n}}$ and $\hat{\mathbf{z}}$ are orthogonal unit vectors in the direction normal to the local flow velocity and in the spanwise direction respectively.

The transport equation for the vorticity is given by the vorticity equation, which can be linearized about a potential mean flow to give

$$(6)$$

$$\frac{D_o\omega}{Dt} - \omega.\nabla\mathbf{U} = 0$$

The solution to this equation can be obtained in terms of the drift coordinates X_i which are solutions to the differential equation

$$(7)$$

$$\frac{D_o}{Dt}(\mathbf{X} - \mathbf{U}^{(\infty)}t) = 0$$

The solution to (6) in terms of drift functions takes the form

$$(8)$$

$$\frac{\partial X_j}{\partial x_i}\omega_i = \omega_j^{(\infty)}$$

where $\omega_j^{(\infty)} = \omega_j^{(\infty)}(\mathbf{X} - \mathbf{U}^{(\infty)}t)$ is the vorticity in a volume V_T which lies well upstream of the blade in a region of uniform flow of mean velocity $\mathbf{U}^{(\infty)}$. We specify the vector components (x_1,x_2,x_3) such that x_1 is parallel to the mean flow $\mathbf{U}^{(\infty)}$, x_2 is normal to the mean flow, and x_3 is in the spanwise direction. The gradients of the drift functions X_2 and X_3 are given by

$$(9)$$

$$\nabla X_2 = \frac{U}{U_\infty}\hat{\mathbf{n}} \qquad \nabla X_3 = \hat{\mathbf{z}}$$

and so the Lamb vector can be evaluated using (5) and (9) as

$$(10)$$

$$(\omega \times \mathbf{U}) = U_\infty\omega_2^{(\infty)}\hat{\mathbf{z}} + U\omega_3^{(\infty)}\hat{\mathbf{n}}$$

32

This is an important result because it shows how the source term for the boundary element method can be specified in terms of the vorticity far upstream of the blade where the mean flow is uniform. The Lamb vector has two components, one that is in the spanwise direction and one that is normal to the span. Further simplification is possible if we limit consideration to the net unsteady loading on the blade, which can be obtained from the spanwise integral of the potential given by (4). We find

(11)

$$
\int_{span} \dot{\varphi}(\mathbf{x}) H(f) dx_3 = \int_{span} \int_{V_e} U_\infty \omega_2^{(\infty)}(\mathbf{X}(\mathbf{y}) - \mathbf{U}^{(\infty)}t) \frac{(y_3 - x_3)}{4\pi |\mathbf{y} - \mathbf{x}|^2} dV(\mathbf{y}) dx_3
$$

$$
+ \int_{span} \int_{V_e} U\omega_3^{(\infty)}(\mathbf{X}(\mathbf{y}) - \mathbf{U}^{(\infty)}t) \frac{(\mathbf{y} - \mathbf{x}).\hat{\mathbf{n}}}{4\pi |\mathbf{y} - \mathbf{x}|^2} dV(\mathbf{y}) dx_3
$$

$$
+ \int_{span} \int_{S} \dot{\varphi}(\mathbf{y}) \frac{(\mathbf{y} - \mathbf{x}).\hat{\mathbf{n}}}{4\pi |\mathbf{y} - \mathbf{x}|^2} dS(\mathbf{y}) dx_3
$$

For blades of infinite span for which end effects are negligible the first integral on the right hand side of (11) is zero because for each value of y_3 the integrand over x_3 is zero. The panel source strength when integrated over the span will therefore only depend on the spanwise component of the vorticity. Hence the unsteady loading, which is derived from the panel source strength, will also only depend on ω_3. The problem of modeling a turbulent inflow for numerical calculations is therefore greatly simplified because only one component of the vorticity contributes to the unsteady lift. Calculating the blade response to the spanwise component of a vortical gust will give all the information required to specify the response to a more general vortical gust.

Another feature of this result is that the unsteady loading on the blade can be calculated from the response of a two dimensional airfoil to the spanwise average of the spanwise vorticity component. This greatly simplifies the numerical cost of doing the calculation for the unsteady loading, which can be important for high frequency noise calculations, even for very simple systems. The analytical method given in Part A can be used for this purpose, and the numerical results presented here were computed using this approach because it was numerically more efficient, and the results agreed closely with the calculations based on the boundary element method.

3.0 Blade Turbulence Interactions

The problem of applying boundary element methods to turbulent flows identified by Grace[2] is greatly reduced by using the results of the analysis above. For blades of large span in a uniform mean flow we have shown that the unsteady loading can be calculated from the spanwise average of the spanwise vorticity component and the response to a two dimensional blade vortex interaction. In this section we will show how the response function can be coupled to the wavenumber spectrum of the upstream turbulence.

Following the approach used by Amiet[3] the unsteady loading caused by a turbulent inflow can be obtained from the response of the blade to a harmonic gust. In general the vorticity in the flow can be expressed in terms of its wavenumber transform

(12)

$$\omega_3^{(\infty)}(\mathbf{x},t) = \int_{-\infty}^{\infty} \int_{-\infty}^{\infty} \int_{-\infty}^{\infty} a(k_1,k_2,k_3)e^{-ik_1(x_1-U_\infty t)-ik_2x_2-ik_3x_3} dk_1 dk_2 dk_3$$

in the region of flow far upstream of the blade where the flow is uniform. Since the response is linear the unsteady loading can be obtained by superimposing the response of the blade to harmonic gusts of amplitude $a(k_1,k_2,k_3)$. The unsteady loading depends on the spanwise average of the vorticity, which for each harmonic component will be $2\pi a(k_1,k_2,k_3)\delta(k_3)\exp(-ik_1(x_1-U_\infty t)-ik_2x_2)$. If the unsteady loading in response to a harmonic gust is $S(k_1,k_2)$, then the time history of the complete response is

(13)

$$L(t) = 2\pi \int_{-\infty}^{\infty} \int_{-\infty}^{\infty} a(k_1,k_2,0)S(k_1,k_2)e^{ik_1U_\infty t} dk_1 dk_2$$

and the loading in the frequency domain is

(14)

$$\tilde{L}(\omega) = \frac{2\pi}{U_\infty} \int_{-\infty}^{\infty} a(k_o,k_2,0)S(k_o,k_2)dk_2$$

with $k_o = -\omega/U_\infty$. For time domain calculations it is more numerically efficient to consider a gust of the form

(15)

$$\exp(-ik'_2 x_2)\delta(x_1-U_\infty t)$$

which has the wavenumber transform $a(k_o,k_2,0)=2R_3\delta(k_2-k'_2)/(2\pi)^2$ where $2R_3$ is the span of the blade. The time history of the unsteady loading from this gust is given by

(16)

$$L_\tau(t,k_2) = \frac{2R_3}{2\pi} \int_{-\infty}^{\infty} S(k_1,k_2)e^{ik_1U_\infty t} dk_1$$

and taking the Fourier transform of this with respect to time gives

(17)

$$\tilde{L}_\tau(\omega,k_2) = \frac{2R_3}{2\pi U_\infty}S(k_o,k_2)$$

The unsteady loading in the frequency domain can then be calculated as

(18)

$$\tilde{L}(\omega) = (2\pi)^2 \int_{-\infty}^{\infty} \frac{a(k_o,k_2,0)\tilde{L}_\tau(\omega,k_2)}{2R_3} dk_2$$

This leads to the unsteady loading spectrum which is defined as

(19)

34

$$S_{LL}(\omega) = \frac{\pi}{T} Ex\left[|\tilde{L}(\omega)|^2\right] = (2\pi)^4 \int_{-\infty}^{\infty} \int_{-\infty}^{\infty} \frac{\pi}{T} Ex\left[a(k_o,k_2,0)a^*(k_o,k'_2,0)\right]\frac{|\tilde{L}_r(\omega,k_2)|^2}{(2R_3)^2} dk_2 dk'_2$$

The turbulence is defined in a region of dimension $2R_1 x 2R_2 x 2R_3$ and the averaging time is $2T=2R_1/U_\infty$ we can simplify this integral using

(20)

$$\frac{\pi^2}{R_1 R_3} Ex\left[a(k_o,k_2,0)a^*(k_o,k'_2,0)\right] = \Omega_{33}(k_o,k_2,0)\delta(k_2-k'_2)$$

where Ω_{33} is the wavenumber spectrum of the vorticity which can be defined in terms of the energy spectrum of the turbulence, $\Omega_{33}(k_o,k_2,0)=E(k)/4\pi$ with $k=(k_o^2+k_2^2)^{1/2}$ ($E(k)$ is given for example by Amiet[3]). The final result is

(21)

$$S_{LL}(\omega) = 16\pi^3 U_\infty R_3 \int_{-\infty}^{\infty} \Omega_{33}(k_o,k_2,0)\frac{|\tilde{L}_r(\omega,k_2)|^2}{(2R_3)^2} dk_2$$

The far field noise is calculated from the unsteady loading spectrum in the usual way giving, at a distance r from the blade, and at an angle θ to the direction of the unsteady loading, the sound spectrum as $S_{pp}(\omega)=(\omega\cos\theta/4\pi rc_o)^2 S_{LL}(\omega)$ where c_o is the speed of sound.

The procedure for calculating the far field sound is therefore to compute the unsteady loading time history for a two dimensional blade (which gives the unsteady loading per unit span) for a set of elemental vortices which are initiated at different heights x_2 above the stagnation streamline and convected past the blade. The resulting time histories are Fourier transformed with respect to time and multiplied by $\exp(-ik_2x_2)$ and integrated over x_2 to obtain $\tilde{L}_r(\omega,k_2)/2R_3$. The result is then used in (21) to obtain the unsteady loading spectrum.

4.0 Numerical Results

In order to verify the numerical accuracy of the procedures described in the previous sections a test was carried out to compare the broadband noise spectrum calculated numerically with the analytical calculation for a flat plate given by Amiet[3]. The numerical calculation was carried out for an airfoil with 1% thickness to chord ratio and zero angle of attack. The blade chord is 0.91m and the turbulence lengthscale was 0.0912 of the blade chord. The flow speed was 30m/s and the turbulence intensity was 4%. The results of this calculation are shown in Fig. 1 and give the 1/3rd octave band Sound Pressure Level of the radiated noise (narrow band spectra, given by (19), have been corrected by a factor of $2(0.23\omega)$ to account for the $1/3^{rd}$ octave band filter). Results are presented as Sound Pressure Levels in dB re 20 microPa measured directly above the airfoil at a distance of 1.82m. The time stepping on for the lift response calculation is given in non-dimensional steps of $2\Delta t U/c=0.0037$ for 16392 points, and 200 discrete vortex elements were equally spaced from one chord above the stagnation streamline to

one chord below the stagnation streamline. The results indicate that for this example the numerical method is accurate, with a small error at high frequencies.
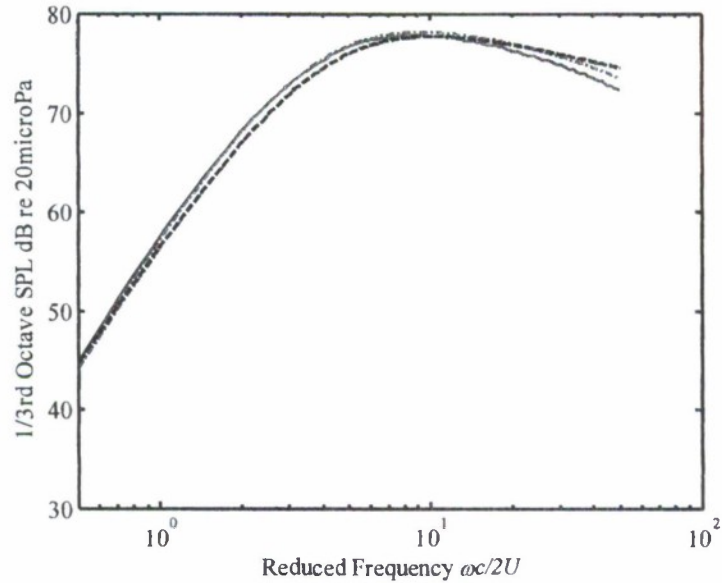

Figure 1: Numerical calculations for a flat plate compared to Amiets theory for a turbulent inflow with an integral lengthscale *L/c=0.0922*. *solid line*:numerical calculation, ---- Amiets theory, -.-.-. numerical calculation using time history of upwash gust.
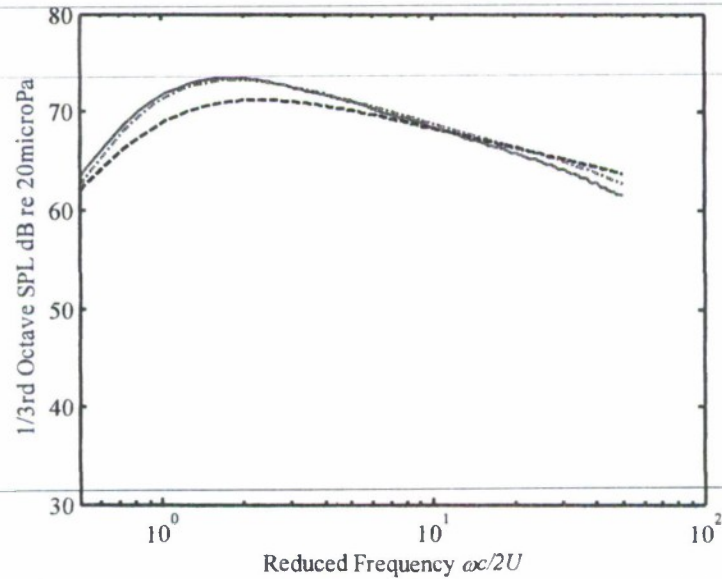

Figure 2: Numerical calculations for a flat plate compared to Amiets theory for a turbulent inflow with an integral lengthscale *L/c=0.415*. *solid line:* numerical calculation, ---- Amiets theory, -.-.-. numerical calculation using time history of upwash gust.

However if all parameters remain the same and the chord is reduced to 0.2m, so the turbulence lengthscale becomes 0.415 of the blade chord, then the accuracy of the

36

numerical calculation is reduced as shown in Fig. 2. The errors occur at low frequencies and cause a predicted level which exceeds the analytical level by a few dB. Also shown in Figs 1 and 2 are the numerical calculations of the radiated noise obtained from the time history of the upwash gust at the leading edge of the blade induced by the array of discrete vortices. Numerically Fourier transforming the upwash gust and multiplying it by Sears function gives the unsteady loading for each vortex element. The analysis in section 3 can then be used to calculate the radiated noise and provides a method for identifying if the source of the numerical error is from the unsteady loading calculation or the modeling of the gust. This calculation agrees with the calculation based on the full numerical evaluation of the unsteady pressure, and so we conclude that the source of the numerical error is due to the modeling of the gust, not the calculation of the blade response.

To show the effect of angle of attack and blade thickness on the radiated noise calculations were carried out for an airfoil with a thickness to chord ratio of 12% at angle of attack of 0 deg and 10 deg. The results, shown in Fig. 3 for the parameters used in Fig. 1, demonstrate that the effect of angle of attack is small, but that the effect of blade thickness is to reduce the spectral level at high frequencies by a large amount. This result is consistent with the analytical results of Howe[6], Gerschfeld[7] and Part A of this report but we believe that this is the first time that this calculation has been done for a real airfoil shape in a turbulent flow. The physical explanation for these effects are given in Part A of this report who show that the effect of angle of attack on the response of an airfoil to a symmetric gust is to rotate the direction of the unsteady loading vector with out altering its magnitude.
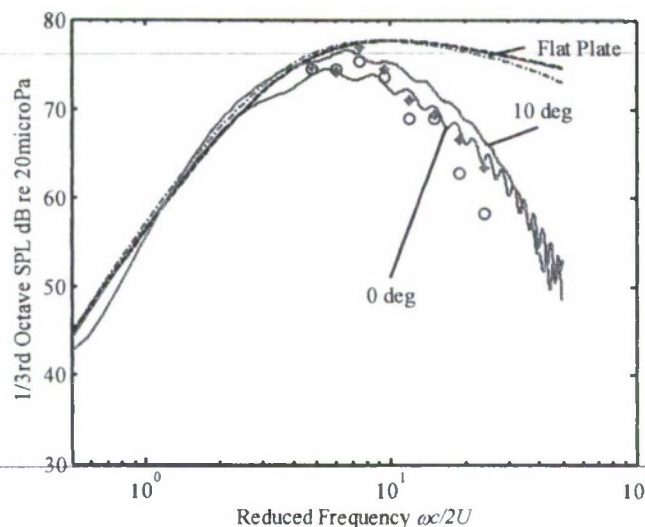

Figure 3: The third octave spectra for the 36" NACA 0012 airfoil. o measured data for 0 deg angle of attack, * measured data for 10deg angle of attack, lines show predicted levels for 12% thick airfoils and Amiet's theory for a flat plate.

The numerical results shown in Fig. 3 confirm this finding. In contrast the analytical results show that the effect of increasing the blade thickness is to smooth the blade

response as the gust passes the leading edge of the airfoil, and this reduces the high frequency content of the loading noise, as indicated in Fig. 3.

5.0 Comparison With Experimental Measurements

Calculations of the unsteady loading on several different airfoils have been compared with new wind tunnel measurements taken in the Virginia Tech Stability Wind Tunnel. The wind tunnel combines a large test section (6' x 6' x 24') and wide speed range (0 to 80m/s). The facility can be configured for aerodynamic measurements in a hard-wall test section or in aeroacoustic configuration which includes an acoustically treated half open jet test section and surrounding anechoic chamber (26' x 18' x 12'). In aeroacoustic configuration the facility is capable of running a conventional jet catcher system, but it is normally configured to use large Kevlar acoustic windows to contain the jet flow while allowing acoustic transmission into the anechoic chamber. The Kevlar walls allow near and far-field acoustic measurements with much less aerodynamic interference than is present in open jet configuration. Other acoustic window materials, such as polypropylene mesh and light impermeable nylon can also be mounted. A full description of these measurements are presented in [13].

Measurements were made of the far field radiated noise for five different airfoils with thickness to chord ratios of 12% and 15%, with 0.203m, 0.610m and 0.914m chords. The inflow turbulence had a lengthscale of 0.084m in and a turbulence intensity of 4%. The tunnel flow speed was 30 m/s, and the acoustic measurements were made 1.8m directly above the airfoil (as in the example discussed in section 4). Note that the measured spectra may reflect some influence of the response of the anechoic chambers below 150Hz which has not yet been corrected for. This corresponds to reduced frequencies of 3 and 14 for the 0.203 and 0.914-m chord foils respectively.

Fig. 3 shows the comparison of the calculations with the measurements for the 12% thick NACA 0012 airfoil with a chord of 0.912m for angles of attack 0 deg and 10deg. The measurements agree well with the numerical calculations, and although there is a small error the measurements confirm the reduction of high frequency sound levels for the 12% thick airfoil compared to the flat plate. For non dimensional frequencies above 10 this reduction is substantial.

To confirm these results Fig. 4 shows the measurements and calculations for a NACA 0012 airfoil with a chord of 0.203m. In this case the angle of attack at high frequencies does not appear to have any effect, and the measured change in level is predicted by the numerical calculations. However the absolute level prediction is not as good as for the large airfoil, but the differences between the measurements and the predictions are consistent with the numerical computation error discussed in section 4.
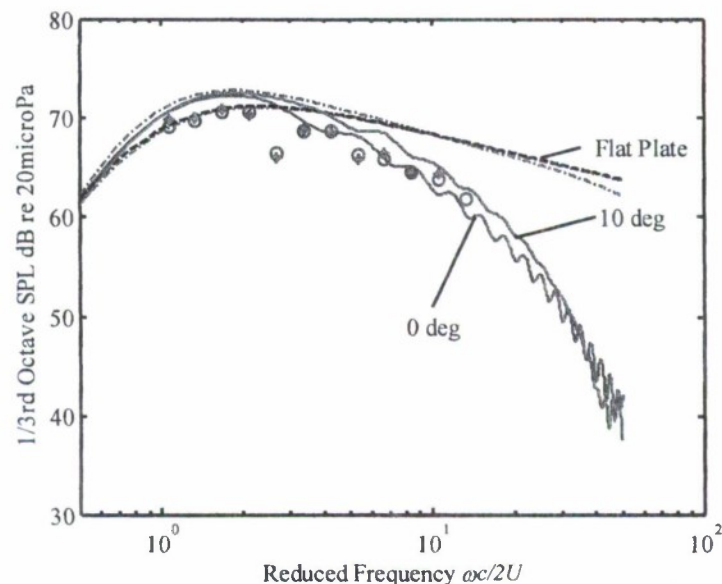
Figure 4:The third octave spectra for the 8" NACA 0012 airfoil. o measured data for 0 deg angle of attack, * measured data for 8deg angle of attack, lines show predicted levels for 12% thick airfoils and Amiet's theory for a flat plate

6.0 Conclusions

This paper has considered the prediction of broadband noise from airfoils of arbitrary shape subject to a turbulent inflow. It has been shown how a time domain approach based on a boundary element method can be used to predict the radiated noise. An important feature is the simplification of the inflow turbulence description for blades of large span in a uniform potential flow. It was shown that only the spanwise average of the spanwise component of the inflow vorticity is required to make far field noise predictions, and that a two dimensional blade response code could be used.

Numerical calculation were compared to wind tunnel measurements with some success and it was shown both experimentally and numerically that the effect of angle of attack on the radiated noise level was very small. However blade thickness reduces the high frequency content of the blade response and hence the high frequency content of the radiated noise spectrum.

References

[1] Rockwell, D., Vortex body interactions, Annual Review of Fluid Mechanics, 30:pp199-229, 1998.

[2] Grace S M, Unsteady Blade Response: The BVI Model vs. the Gust Model, *Proceedings of the 7th AIAA/CEAS Aeroacoustics Conference*, Maastricht, AIAA paper no 2001-2209, 2001

[3] Amiet, R.K., Acoustic Radiation from an airfoil in a turbulent stream, J. Sound and Vibration, vol 41(4), pp 407-420, 1975

[4] Atassi, H. M. The Sears problem for a lifting airfoil revisited new results. *Journal of*

Fluid Mechanics 141, 109-122., 1984

[5] Myers M.R. and Kerschen E.J., Influence of incidence angle on sound generation by airfoils interacting with high frequency gusts, J. Fluid Mechanics, Vol 292, pp271-304, 1995

[6] Howe, M.S., "Correlation of lift and thickness noise sources in vortex airfoil interactions", J. Sound and Vibration, Vol 137(1), pp 1-7, 1990.

[7] Gershfeld, J., Leading edge noise from thick airfoils in turbulent flows, J. Acoustical Soc. Am. vol 116(3), pp1416-1426, 2004.

[8] Lockard D.P. and Morris P.J. , Radiated Noise from airfoils in realistic mean flows, AIAA Journal, Vol 36, nO 6, PP 907-914, 1998

[9] Katz J. and Plotkin, A., Low Speed Aerodynamics, 2nd ed, Cambridge university Press, 2000

[10] Glegg, S, and Devenport W., Unsteady Loading from Airfoils of Arbitrary Thickness. *Submitted to the Journal of Sound and Vibration*

[11] Staubs J., Devenport W., and. Glegg, S., Real airfoil effects on sound radiated from airfoils immersed in grid generated turbulence, *AIAA Paper No 2008-3018 presented at the AIAA Aeroacoustics conference, Vancouver, May 2008*